Redox Biology 76 (2024) 103335

Contents lists available at ScienceDirect

Redox Biology

journal homepage: www.elsevier.com/locate/redox

Oxidative stress promotes oral carcinogenesis via Thbs1-mediated M1-like tumor-associated macrophages polarization

Wei Li [a,b,1], Qingwen Zeng [a,b,1], Bing Wang [a,b,1], Chao Lv [a,b], Haoan He [a,b], Xi Yang [c,**], Bin Cheng [a,b,***], Xiaoan Tao [a,b,*]

[a] Hospital of Stomatology, Guanghua School of Stomatology, Sun Yat-sen University, Guangzhou, China
[b] Guangdong Provincial Key Laboratory of Stomatology, Guangzhou, China
[c] Department of Periodontology, Stomatological Hospital, Southern Medical University, Guangzhou, China

ARTICLE INFO

Keywords:
ROS
ASCT2
Thbs1
Macrophages
Oral carcinogenesis

ABSTRACT

Although oxidative stress is closely associated with tumor invasion and metastasis, its' exact role and mechanism in the initial stage of oral cancer remain ambiguous. Glutamine uptake mediated by alanine-serine-cysteine transporter 2 (ASCT2) participates in glutathione synthesis to resolve oxidative stress. Currently, we firstly found that ASCT2 deletion caused oxidative stress in oral mucosa and promoted oral carcinogenesis induced by 4-Nitroquinoline-1-oxide (4-NQO) using transgenic mice of ASCT2 knockout in oral epithelium. Subsequently, we identified an upregulated gene Thbs1 linked to macrophage infiltration by mRNA sequencing and immunohistochemistry. Importantly, multiplex immunohistochemistry showed M1-like tumor-associated macrophages (TAMs) were enriched in cancerous area. Mechanically, targeted ASCT2 effectively curbed glutamine uptake and caused intracellular reactive oxygen species (ROS) accumulation, which upregulated Thbs1 in oral keratinocytes and then activated p38, Akt and SAPK/JNK signaling to polarize M1-like TAMs via exosome-transferred pathway. Moreover, we demonstrated M1-like TAMs promoted malignant progression of oral squamous cell carcinoma (OSCC) both in *vitro* and in *vivo* by a DOK transformed cell line induced by 4-NQO. All these results establish that oxidative stress triggered by ASCT2 deletion promotes oral carcinogenesis through Thbs1-mediated M1 polarization, and indicate that restore redox homeostasis is a new approach to prevent malignant progression of oral potentially malignant disorders.

1. Introduction

Oxidative stress is defined as deregulation of reactive oxygen species (ROS) production and ROS limitation, characterized by unspecific oxidation of biomolecules and alteration of normal physiological function. Aberrant redox homeostasis plays important roles in regulating diverse aspects of cell behavior (e.g., proliferation, differentiation, migration and angiogenesis) [1]. It has been proven that oxidative stress is closely associated with tumor progression. On the one hand, oxidative stress triggers tumor development by causing DNA damage and genomic instability [2,3]; on the other hand, the rapid growth of tumor enhances ROS production [4,5]. However, it remains obscure on the role and

Abbreviations: **ASCT2**, alanine-serine-cysteine transporter 2; **SLC**, solute carrier; **4-NQO**, 4-Nitroquinoline-1-oxide; **TAMs**, tumor-associated macrophages; **ROS**, reactive oxygen species; **OSCC**, oral squamous cell carcinoma; **Gln**, glutamine; **TCA**, tricarboxylic acid; **GSH**, glutathione; **OLK**, oral leukoplakia; **OPMDs**, oral potentially malignant disorders; **DOK**, dysplastic oral keratinocytes; **FBS**, fetal bovine serum; **HE**, hematoxylin-eosin staining; **IHC**, immunohistochemistry staining; **IF**, immunofluorescence staining; **mIHC**, multiplex immunohistochemistry staining; **DHE**, dihydroethidium; **FPKMs**, fragments per kb of transcript per million reads; **DEGs**, differentially expressed genes; **GO**, gene ontology enrichment; **KEGG**, kyoto encyclopedia of genes and genomes; **HNSCC**, head and neck squamous cell carcinoma; **qPCR**, quantitative real-time PCR; **TEM**, transmission electron microscopy; **nanoFCM**, nano flow cytometry; **GSSG**, oxidized glutathione; **TME**, tumor immune microenvironment; **NAC**, N-acetylcysteine; **CM**, conditioned medium.

* Corresponding author. Hospital of Stomatology, Sun Yat-sen University, No.56, Lingyuan Xi Road, Guangzhou, 510055, Guangdong, China.
** Corresponding author.
*** Corresponding author. Hospital of Stomatology, Sun Yat-sen University, No.56, Lingyuan Xi Road, Guangzhou, 510055, Guangdong, China.
E-mail addresses: yangxi53@126.com (X. Yang), Chengbin@mail.sysu.edu.cn (B. Cheng), taoxiaoa@mail.sysu.edu.cn (X. Tao).
[1] These authors contributed equally to this work.

https://doi.org/10.1016/j.redox.2024.103335
Received 24 April 2024; Received in revised form 6 July 2024; Accepted 29 August 2024
Available online 5 September 2024

mechanism of oxidative stress in the initiation of tumor carcinogenesis.

Glutamine (Gln) is the most abundant and widely used non-essential amino acid in the human body, which involves in tricarboxylic acid (TCA) cycle and inter-organ nitrogen exchange [6]. In addition, Gln can balance redox homeostasis by participating in de novo biosynthesis of glutathione (GSH) to cope with oxidative stress [7–9]. Alanine-serine-cysteine transporter 2 (ASCT2, encoded by gene Slc1a5) has been acknowledged as the major Gln transporter [10,11], although there have been numerous membrane transporters generally recognized as four Solute Carrier (SLC) families (SLC1, SLC6, SLC7 and SLC38) [12,13]. ASCT2 is an obligatory Na^+-dependent amino acid transporter which mediates the cotransport of Na^+ with Gln or other neutral amino acids (alanine, serine and cysteine) to support the biosynthetic pathways [12,14]. There have been numerous studies showed that targeted interference with ASCT2-mediated Gln uptake significantly suppressed Gln metabolism, especially GSH production, which contributed to redox imbalance and induced cellular oxidative stress [15–18].

Oral leukoplakia (OLK) is one of the most common oral potentially malignant disorders (OPMDs) in oral mucosa and has the potential to develop into oral squamous cell carcinoma (OSCC) which affects nearly 377713 people worldwide in 2020 [19–21]. Although the etiology and anatomical locations are varied, a hallmark of OSCC is redox imbalance characterized by decreased antioxidant and increased oxidant [22,23]. 4-Nitroquinoline-1-oxide (4-NQO) is a synthetic quinolone-derived molecule which is used to mimic the carcinogenic effect of tobacco [21,24]. It can induce intracellular oxidative stress, leading to the production of ROS metabolic substances that bind to DNA and generating DNA adducts [24,25]. So far, the 4-NQO-induced mouse model remains the most ideal model that accurately reflects the process of oral carcinogenesis.

In current study, we firstly induced oxidative stress in oral mucosa by utilizing ASCT2 conditional knockout mice, and subsequently found that oxidative stress promoted oral mucosa carcinogenesis. Mechanically, it was associated with the polarization of M1-like tumor-associated macrophages (TAMs) activated by exosome-transferred Thbs1. Altogether, the results established restoring redox homeostasis as a new approach targeting ROS-Thbs1-M1 pathway to prevent oral carcinogenesis.

2. Materials and method

2.1. Transformation of human dysplastic oral keratinocyte cells by 4-NQO and RNA transfection

The human dysplastic oral keratinocytes (DOK) were obtained from Dr. Juan Xia (Hospital of Stomatology, Guanghua School of Stomatology, Sun Yat-sen University). DOK cells were cultured in high-glucose DMEM (Gibco, NY, USA) supplemented with 10 % fetal bovine serum (FBS, Gibco, NY, USA) and 5 μg/mL hydrocortisone (Sigma-Aldrich, St. Louis, MO, USA).

DOK cells were transformed by 4-NQO (Sigma-Aldrich, St. Louis, MO, USA) in our laboratory. Cultures were exposed to 2.6 μM 4-NQO for 3 h as described previously [26]. After passed 30 generations of intermittently 4-NQO-treatment over 2 months, the DOK-4-NQO cells were expanded for tumorgenicity *in vitro* and *in vivo*.

To generate stable silenced DOK cells, shRNA lentiviral vectors targeting ASCT2 were purchased from Genechem Co., Ltd (Shanghai, China) and transfected into DOK cells with corresponding control vectors according to the manufacturer's protocols. After transfection, DOK cells were incubated in conditioned medium (CM) with 2 μg/mL puromycin (Aladdin Co., Ltd, Shanghai, China) to select the stably transfected cells. The sequences of the shRNAs were presented in Table S1 (Supporting information).

To determine the function of Thbs1 in ASCT2 knockdown DOK cells, small interfering RNA (siRNA) oligonucleotide (Hanbio Co., Ltd, Shanghai, China) was used. RNAFit Transfection Reagent (Hanbio Co., Ltd, Shanghai, China) was used to facilitate the transfection of siRNA oligonucleotides into the targeted cells in accordance with manufacturer's instruction. The Thbs1 siRNA sequences were listed in Table S1 (Supporting information).

2.2. Human macrophage differentiation in vitro

The human monocyte cells THP-1 were provided as a gift from Dr. Zhengmei Lin (Hospital of Stomatology, Guanghua School of Stomatology, Sun Yat-sen University). THP-1 cells were maintained in RPMI 1640 medium (Gibco, NY, USA) with 10 % FBS and 5 mM β-mercaptoethanol (Macklin Co., Ltd, Shanghai, China). M0 macrophages were differentiated from THP-1 cells using 100 ng/mL phorbol 12-myristate 13-acetate (PMA, Sigma-Aldrich, St. Louis, MO, USA) for 48 h. Then, the THP-1-derived macrophages were further differentiated into M1-like cells cultured in medium with 20 ng/mL IFN-γ (PeproTech Inc., NJ, USA) and 100 ng/mL LPS (Absin Bioscience Inc., Shanghai, China), or differentiated into M2-like cells cultured in medium with 20 ng/mL IL-4 (PeproTech Inc., NJ, USA) and 20 ng/mL IL-13 (PeproTech Inc., NJ, USA) for 48 h. To obtain conditioned medium (CM) of M0 or M1 macrophages, cells, about 70%–80 % confluence were washed and cultured for additional 24 h with fresh RPMI 1640 medium with 10 % FBS and 5 mM β-mercaptoethanol. Then the supernatants were centrifuged at 3000 g (4 °C) for 15 min and finally were filtrated through 0.22 μm Filter Units (Merk Millipore, MA, USA).

2.3. Animal models

$Slc1a5^{tm1.1cyagen}$ mice (CKOCMP'-02923-Slc1a5) were purchased from Cyagen Biosciences Inc (SF, USA). K14-$CreER^{tam}$ mice (JAX-005107) were kindly given as a gift by Dr. Juan Xia (Hospital of Stomatology, Guanghua School of Stomatology, Sun Yat-sen University), which expressed Cre recombinase in squamous epithelium under the control of the K14 promoter. $Slc1a5^{f/f}$ Cre $^{\pm}$ mice were generated by crossing the floxed Slc1a5 allele $Slc1a5^{tm1.1cyagen}$ ($Slc1a5^{f/f}$) mice with K14-$CreER^{tam}$ (K14-$Cre^{+/-}$) mice. Genotype of transgenic mice were identified by the One Step Geno Typing Kit (Vazyme Biotech Co, Nanjing, China) following the manufacturer's protocol.

For acquiring Slc1a5 conditional knockout mice, $Slc1a5^{f/f}$ Cre $^{\pm}$ mice were intraperitoneally injected with tamoxifen (TAM, Sigma Aldrich, St. Louis, MO, USA) five times every other day at a dose of 120 mg/kg. The PCR primers of genotyping were provided in Table S2 (Supporting information).

For mouse model of 4-NQO-induced oral carcinogenesis, 4-NQO was dissolved in propylene glycol (Macklin, Shanghai, China) to prepare stock solution (1 mg/mL) and further diluted to working solution (100 μg/mL) in drinking water every week. For inducing oral carcinogenesis, mice with the same gene background ($Slc1a5^{f/f}$ $Cre^{+/-}$) were fed with working solution for 16 weeks and maintained with regular drinking water for a further 6 weeks. All animal experiments were approved by the Laboratory Animals Ethics Committee of Sun Yat-sen University (SYSU-IACUC-2019-000228).

For xenograft model, male BALB/c nude mice (nu/nu, aged 3–5weeks) were purchased from the Laboratory Animal Center of Sun Yat-sen University (Guangzhou, China). In brief, $1*10^6$ DOK or DOK-4-NQO cells/per site were subcutaneously injected under the skin of the axillary to establish the nude mouse xenograft tumor models ($n \geq 6$ for each group). For assessing the effects of CM of macrophages on the tumorigenesis of DOK-4-NQO cells, mice with xenografts were intraperitoneally injected with 500 μL CM from M1-like TAMs, M0 or RPMI 1640 every other day. Tumor volumes (length * $width^2/2$) were monitored and compared. The above animal experiments were approved by the Laboratory Animals Ethics Committee of Sun Yat-sen University (SYSU-IACUC-2023-001462, SYSU-IACUC-2024-000773).

2.4. Histological hematoxylin-eosin (HE) saining and immunohistochemistry (IHC)

For tissue HE staining, tissues were dissected and fixed overnight with 4 % paraformaldehyde (Biosharp, Chongqing, China). Samples were then embedded in paraffin. For the HE staining of cells, cells were just fixed with 4 % paraformaldehyde for 15 min. Paraffin sections with 4 mm thick or cells were prepared and stained with hematoxylin and eosin (Servicebio Co, Ltd, Wuhan, China) for histology. IHC was carried out in accordance with the manufacturer's guidelines of the IHC Kit (Gene Tech, Shanghai, China) and quantified as our previous published methods [17,27]. The antibodies used in IHCassays were listed in Table S3 (Supporting information).

2.5. Western blot

The protocol was conducted according to the previous studies [17,28]. The primary antibodies used were listed in Table S3 (Supporting information). The secondary antibodies were anti-rabbit or anti-mouse HRP-conjugated antibodies (1:5000, EMAR, Beijing, China). The bands were visualized by chemiluminescent HRP substrate (Millipore, MA, USA).

2.6. Tissue immunofluorescence (IF) staining and multiplex IHC (mIHC)

Tissue IF was conducted as previously described [27]. In short, sections were first incubated with primary antibodies against ASCT2, 8-Hydroxyl-2-deoxyguanosine (8-OHdG) or γ-H2AX which was from DNA Damage Assay Kit (C2035S, Beyotime, Shanghai, China). Then these sections were incubated with corresponding fluorochrome-conjugated secondary antibodies for 1 h. Sections were then counterstained with DAPI (Solarbio, Beijing, China) and evaluated in an invert laser confocal microscope (Olympus FV3000, TKY, Japan). mIHC was performed using a Neon DendronFluor Kit (Histova Biotechnology Co, Ltd, Jilin, China) as previously described [27]. The antibodies used in these sections were listed in Table S3 (Supporting information).

2.7. Assessment of oxidative stress in tissue and cells

Visualization of ROS in tongue epithelium samples was conducted by staining for oxidation of cytosolic dihydroethidium (DHE) (Applygen, Beijing, China) as described previously [29]. In brief, 10 μm tongue cryosections were air-dried for 30 min and then incubated with 0.5 μM DHE for 30 min at 37 °C. Then the sections were incubated with primary antibody against ASCT2 overnight at 4 °C, which were followed by incubation with fluorochrome-conjugated secondary antibody Alexa Flour488 for 1 h at room temperature. Sections were next counterstained with DAPI and evaluated in Olympus FV3000. The production of H_2O_2 in tongue mucosa epithelium was assessed by H_2O_2 Content Assay Kit (Solarbio, Beijing, China) according to the manufacture's guideline. GSH/GSSG ratio in tongue mucosa epithelium was determined by using GSH and GSSG Assay Kit (Beyotime, Shanghai, China) as the instruction described. For assessing ROS level in cells, intracellular ROS were detected using the DHE Kit (Applygen, Beijing, China) by flow cytometry as we previously described [17,27].

2.8. RNA sequencing analysis

For mouse model of 4-NQO-induced oral carcinogenesis, mouse tongues were treated with dispase II enzyme (Roche, Basel, Switzerland) to obtain tongue mucosa epithelium for RNA-Seq analysis, which was conducted at OE biotech Co., Ltd. (Shanghai, China). The libraries were sequenced on an Illumina HiSeq X Ten system and 125/150bp paired-end reads were generated. Raw data (raw reads) of the fastq format were first processed using Trimmomatic. Then about 40–55 million clean reads for each sample were acquired by abolishing reads containing adapter or ploy-N and low-quality reads. The clean reads were next mapped to the human genome using HISAT2. The fragments per kb of transcript per million reads (FPKMs) value of each gene were calculated using Cufflinks, and the read counts of each gene were obtained by HTSeq-count. Differentially expressed genes (DEGs) analysis was performed using the DESeq (2012) R package. A P value of <0.05 and a fold change of >2 or <0.5 were set as the threshold for significantly differential expression. Hierarchical cluster analysis of differentially expressed genes was conducted to analyze transcript expression patterns. Gene ontology enrichment (GO) and Kyoto Encyclopedia of Genes and Genomes (KEGG) pathway enrichment analysis of DEGs were performed using R based on the hypergeometric distribution.

2.9. Bioinformatics analysis

Bioinformatics analysis was conducted on the basis of the TCGA cohort of head and neck squamous cell carcinoma (HNSCC). Gene expression data of corresponding number pairs of adjacent and cancer samples was extracted to analyze the Thbs1 expression in HNSCC samples. The survival data was analyzed using the "survival" (v3.3.1) R package. K-M survival curve analysis was used to identify the survival outcomes of HNSCC patients based on the Thbs1 expression levels. The ssGSEA algorithm in the "GSVA" (v1.46.0) R package [30] was used to assess the tumor infiltration status of 24 immune cell types [31]. Besides, we used the spearman's correlation analysis to evaluate the relationship between Thbs1 expression level and the immune cell infiltration status.

2.10. Flow cytometry

For cell analysis, Zombie NIR™ Fixable Viability Kit (Biolegend, CA, USA, diluted at 1:500) was used to label dead cells at room temperature for 30 min firstly. Then, cells were incubated with specific antibodies for 30 min on ice. Data was acquired on LSRFortessa (BD Bioscience, NJ, USA) and was analyzed using Flowjo software (BD Bioscience, NJ, USA). The antibodies were listed in Table S3 (Supporting information).

2.11. RNA extraction and quantitative real-time PCR (qPCR)

Total RNA was isolated from cells with RNA-Quick Purification kit (ES Science, Shanghai, China). RNA concentration was measured by NanoDrop One (Thermo Fisher Scientific Inc., CA, USA). HiScript III RT SuperMix for qPCR kit (Vazyme Biotech Co., Nanjing, China) was used to reversed-transcribe 1 μg of RNA to acquire cDNA. Quantitative RT-PCR was conducted to quantify gene expression level of β-actin, ASCT2 and Thbs1 by applying ChamQ Universal SYBR qPCR Master Mix (Vazyme Biotech Co., Nanjing, China) and quantified by $2^{-\Delta\Delta CT}$ method. The primers used in this study, purchased from GeneRay biotechnology (Guangzhou, China) were listed in Table S1 (Supporting information).

2.12. Exosome isolation, characterization and tracing

Exosomes were isolated from the cell culture supernatants by ultracentrifugation. In brief, equal amounts of DOK cells treated differently were seeded on 15-cm dishes and cultured in high glucose DMEM medium with 10 % exosome-free FBS for 48 h. These supernatants were collected and centrifuged at 3000 g for 30 min at 4 °C to abolish dead cells and cell fragments, and then filtered through a 0.22 μm filter (Merk Millipore, MA, USA). Then the solution was ultracentrifuged at 110000 g for 2 h at 4 °C. The precipitate was collected and washed using sterilized PBS (Solarbio, Beijing, China), followed by next ultracentrifugation at 110000 g for 2 h at 4 °C. The pellets of exosome were resuspended with 200 μL PBS.

The morphology and size of exosomes were determined by transmission electron microscopy (TEM, Hitachi, Tokyo, Japan). The size

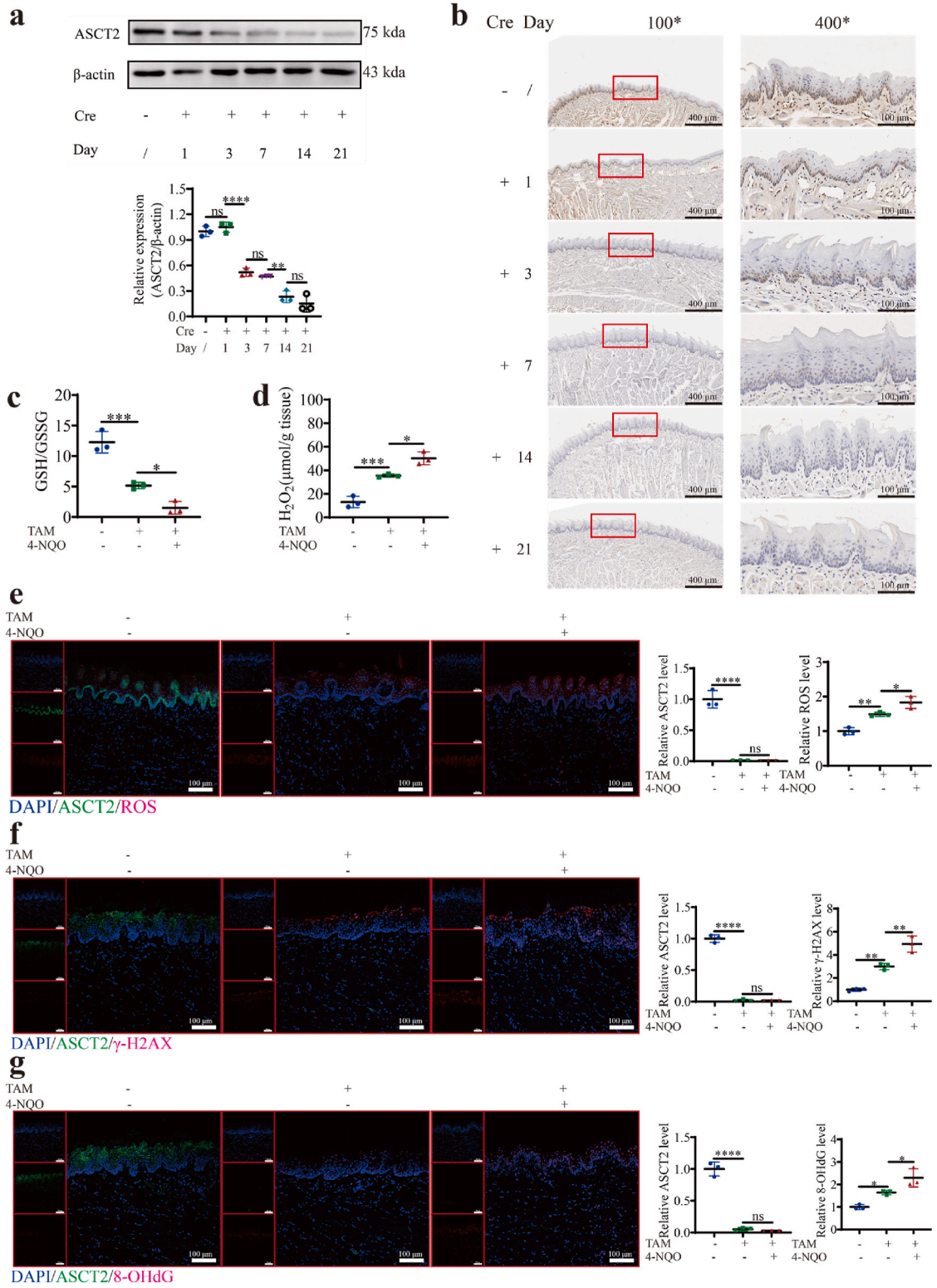

Fig. 1. The identification of oxidative stress in oral mucosa epithelium of ASCT2 knockout mice

Western blot (a) and IHC (b) were used to detect the efficiency of ASCT2 knockout in day 1,3,7,14,21 after tamoxifen injection (120 mg/kg). (Fig. 1–b, magnification × 100 for the left, magnification × 100 for the right, scale bars, 400 μm for 100* magnification and 100 μm for 400* magnification. the red box showed the area of interest). (c) The GSH/GSSG ratio was measured in the 3 groups. (d) H_2O_2 levels were evaluated in oral epithelium using the H_2O_2 Content Assay Kit. (e) ROS levels in oral epithelium of the same gene background ($Slc1a5^{f/f}$ $Cre^{+/-}$) were assessed by DHE staining in cryosections. The markers were ASCT2 (green), ROS (red) and nucleus (blue) respectively. Left: Representative captures from 3 mice for each group. (Scale bar 100 μm). Right: Quantification of ASCT2 and DHE staining using image J. (f) Staining of γ-H2AX of the 3 groups in paraffin sections. The markers were ASCT2 (green), γ-H2AX (red) and nucleus (blue) respectively. Left: Representative captures for each group (Scale bar 100 μm). Right: Quantification of ASCT2 and γ-H2AX staining using image J. (g) Staining of 8-OHdG of the 3 groups in paraffin sections. The markers were ASCT2 (green), 8-OHdG (red) and nucleus (blue) respectively. The above mice used to detect oxidative stress were all male. (For interpretation of the references to colour in this figure legend, the reader is referred to the Web version of this article.)

distribution and concentration were examined by nano flow cytometry (nanoFCM, Agilent, CA, USA). The expression of exosome markers (CD63, CD81, TSG101 and Histone 3) was analyzed by WB. Exosome-tracing experiments were conducted by EvLINK 505 Exosome-labeling Kit (Tingo Regenerative Medicine, Tianjin, China) according to the manufacturer's instruction. Exosomes labeled with fluorescent were incubated with THP-1 cells for 24 h. Then, cells were fixed in 4 % paraformaldehyde and permeabilized in 0.25 % Triton X-100 (Solarbio, Beijing, China) for 30 min respectively. Cells were next incubated with primary antibody against β-Tubulin overnight at 4 °C, followed by incubated with Alex Fluor 594 fluorescent-conjugated secondary antibody for 1 h and counterstained with DAPI. The cells were finally observed by Olympus FV3000. The antibodies were listed in Table S3 (Supporting information). Exosomes were incubated with recipient cells at a concentration of 50 μg exosome protein/10^5 cells in following experiments.

2.13. Glutamine uptake assay

^{3}H-glutamine (Perikin Elmer, MA, USA, NET55120UC) was used to examine glutamine uptake as we previously described [16].

2.14. Metabolite determination

Whole cell lysates of DOK cells were prepared for determined a-ketoglutarate (α-KG), citrate, malate, fumarate and succinate levels using the following ELISA kits: Human a-KG ELISA Kit (Jianglaibio, Co., Ltd, Shanghai, China), Human Citrate ELISA Kit (Jianglaibio, Co., Ltd, Shanghai, China), Human Malate ELISA Kit (Jianglaibio, Co., Ltd, Shanghai, China), Human Fumarate ELISA Kit (Jianglaibio, Co., Ltd, Shanghai, China), and Human Succinate ELISA Kit (Jianglaibio, Co., Ltd, Shanghai, China). The optical density (OD) at 450 nm was examined by a microplate reader and the concentrations were calculated according to respective standard curves. Cellular glutamate, GSH and ATP levels were identified by using Glutamate Assay Kit (Jiancheng Engineering Research Institute, Nanjing, China), Reduced Glutathione Assay Kit (Solarbio, Beijing, China) and ATP Assay Kit (Beyotime, Shanghai, China) respectively according to the manufacturer's instructions.

2.15. Papanicolaou staining assay and cytoskeleton staining assay

The morphology of cells was observed by using Papanicolaou Staining Kit (LBP Medicine Science and Technology Co., Ltd) in accordance with the manufacturer's guideline. For cytoskeleton staining assay, Cells with different treatment were fixed in 4 % paraformaldehyde for 15 min and then permeabilized in 0.25 % Triton X-100 for 30 min at room temperature. The cells were subsequently stained with Actin-Tracker Green-555 (Beyotime, Shanghai, China) for 30 min and counterstained with DAPI. Olympus FV3000 was used for observing.

2.16. Cell cycle assay and cell proliferation assay

For cell cycle assay, DOK cells were seeded on 6-well plates at a density of 2*10^5 per well. Cell Cycle Staining Kit (Multi Sciences, Hangzhou, China) was applied to examine the DNA content of cells in different stages of cell cycle in accordance with the manufacture's instruction. For cell proliferation assay, DOK cells were plated on a 96-well plate at a density of 1*10^3 cell per well and cultured in the corresponding conditions. The cell counting kit-8 solution (CCK-8, Dojindo, Kumanmoto, Japan) was added into wells and incubated for 1 h in a 37 °C incubator in accord with the instruction. the optical density (OD) value was measured at 450 nm and 600 nm.

2.17. Colony formation assay and tumor sphere formation assay

For colony formation assay, 1000 cells/well were seeded in 6-well plates and cultured under the indicated conditions. After incubated for 7 days, cells were fixed with 4 % paraformaldehyde for 15 min, and stained with the crystal violet staining solution (Beyotime, Shanghai, China) for 15 min. The number of colonies (>50 cells) were counted using Image J analysis software. For tumor sphere formation assay, the cells were cultured in ultra-low attachment 96-well plates (Corning Inc., NY, USA) at a density 1000 cells/well in serum-free tumor stem cell medium (TSCM, QIDABIO, Shanghai, China) in a humidified 5 % CO2 incubator at 37 °C. Fresh medium was replenished every 3 days. The number of the valid spheres (>75 μm) was assessed under microscopy 1 week later.

2.18. Cell migration and invasion assay

The *in vitro* cell migration and invasion were measured with the Corning Biocoat Matrigel Invasion Chamber (Corning Inc., NY, USA) according to the manufacturer's instruction. Briefly, 1*10^5 cells resuspended in 200 μL of serum-free medium were seeded in the upper chambers, and 500 μL culture medium with 20 % FBS was added into the lower chambers. After incubated with 24 h, cells of the reverse side of inserts were stained with the crystal violet staining solution and quantified with Image J analysis software.

2.19. Statistical analysis

The results were presented as the mean ± SD from replicated experiments. Two-tailed Student's *t*-test or one-way ANOVA was performed to compare the means of different groups based on the raw data when the data conformed to normal distribution or homogeneity of variance. *P*-values <0.05 were considered statistically significant with Prism 9 (GraphPad Software, San Diego, CA, USA), and the levels of significance were further defined at level of $^*P < 0.05$, $^{**}P < 0.01$, $^{***}P < 0.001$, $^{****}P < 0.0001$.

3. Results

3.1. ASCT2 conditional knockout triggered oxidative stress in oral mucosa

It has been reported *in vitro* that intracellular Gln is mainly converted to glutamate which participates in the synthesis of GSH to protect cells from oxidative stress [15–17,32,33]. However, it remains unknown whether *in vivo* targeted interference with ASCT2-mediated Gln uptake causes redox homeostasis imbalance. We therefore selectively deleted ASCT2 specially in oral mucosa epithelium, as briefly described in Methods (Fig. S1a and b, Supporting information). As shown in Fig. S1c (Supporting information),the tissue-specific gene deletion band (470 bq) was confirmed by the genotyping. The expression of ASCT2 gradually decreased and stabilized 2 weeks after intraperitoneal injection of tamoxifen according to Western blot and IHC experiments (Fig. 1a and b).

We evaluated the production of ROS in the oral mucosa epithelium of mice through five different methodological ways. As shown in Fig. 1c, the oral mucosa epithelium of ASCT2 knockout mice exhibited a lower ratio of reduced GSH to oxidized GSH (GSSG) than control. In addition, the H_2O_2 level was increased after tamoxifen treatment (Fig. 1d). DHE staining was then used to assess the ROS level. ASCT2 deletion also significantly increased the DHE staining (Fig. 1e). Finally, γ-H2AX and 8-OHdG staining showed that treatment with tamoxifen induces DNA oxidation which is an indicator of oxidative stress (Fig. 1f and g). Altogether, these results indicated that ASCT2 deletion promoted the ROS production of oral mucosa epithelium. Interestingly, 4-NQO treatment further increased the ROS level on the basis of ASCT2 knockout.

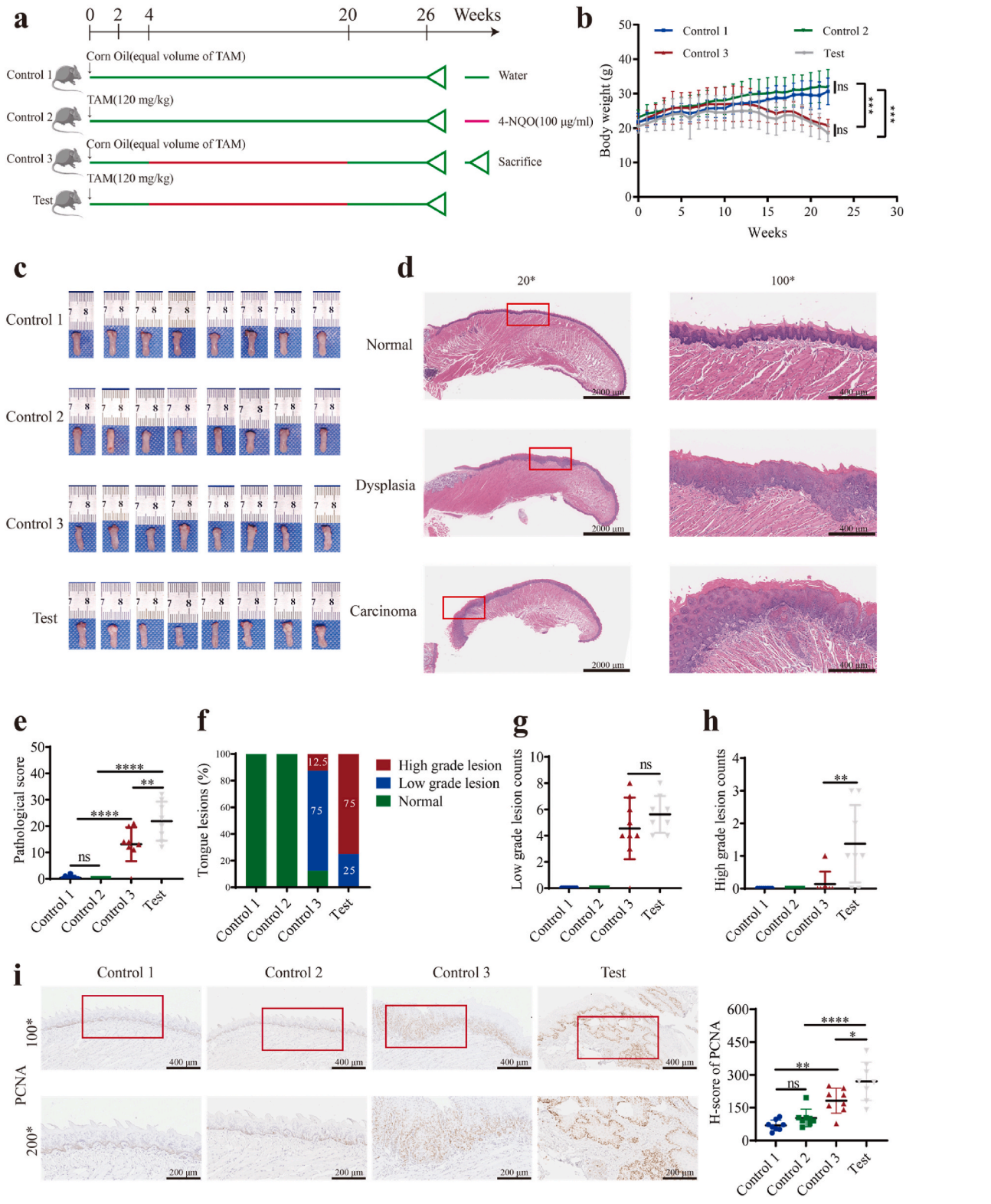

Fig. 2. ASCT2 knockout promoted OSCC occurrence in 4-NQO-treatment mice

(a) Schematic diagram of the experimental strategies *in vivo*. (b) Body weight was recorded every week in different groups. (c) Tongue images of different groups. (d) Representative HE images of normal, dysplasia and carcinoma in tongue. Magnification, 20* and 100*; scale bars, 2000 μm for 20* magnification, 400 μm for 100* magnification. (e) Scores of the histopathologic diagnosis in the four groups. (f) Quantification of the histological ratio of high grade lesion (severe dysplasia and carcinoma), low grade lesion (mild and moderate dysplasia) and normal tissues in the four group. (g) Counts of low grade lesions in the four group. (h) Counts of high grade lesions in the four group. (i) The levels of proliferation cell nuclear antigen (PCNA) were assessed by IHC assay in four groups. Left: Representative images for each group, magnification, 100* and 200*; scale bars, 400 μm for 100* magnification and 200 μm for 200* magnification. The red box showed the area of interest. Right: Quantification of PCNA in the four groups. The above mice were all male and 8 mice for each group. (For interpretation of the references to colour in this figure legend, the reader is referred to the Web version of this article.)

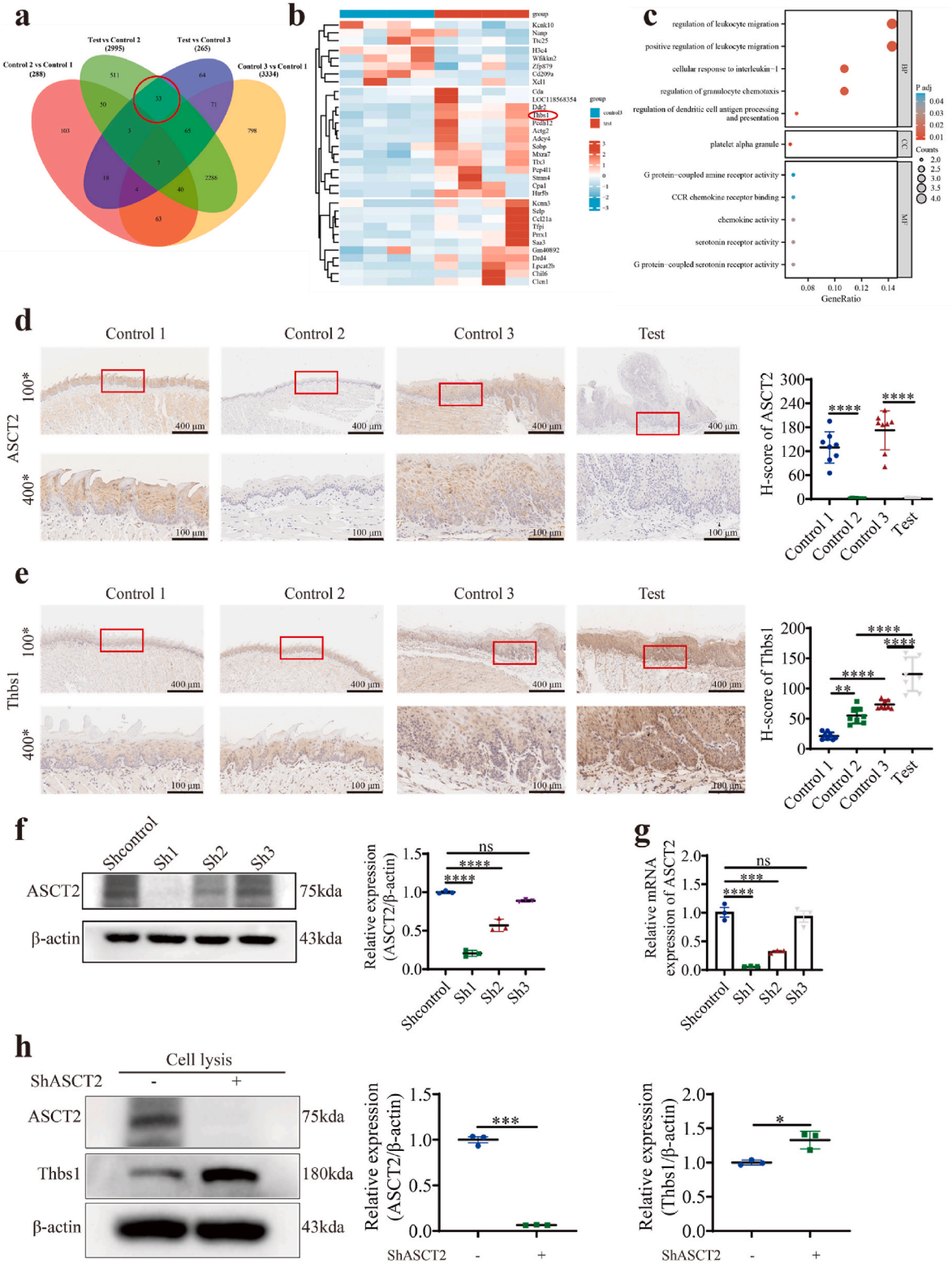

Fig. 3. ASCT2 knockout promoted Thbs1 expression

(a) Venn diagram of differentially expressed genes (DEGs) among the four groups. (b) 33 overlapping genes were clustered to generate a heatmap between control 3 group and test group. (c) GO enrichment plot for the 33 overlapping genes. IHC assay was used to measure the levels of ASCT2 (d) and Thbs1 (e) in the four groups. Left: Representative images for each group, magnification, 100* and 400*; scale bars, 400 μm for 100* magnification and 100 μm for 400* magnification. The red box showed the area of interest. Right: Quantification of ASCT2 and Thbs1 in the four groups. The above mice were all male and 8 mice for each group. (g, h) ASCT2 expression was measured by Western blot and PCR respectively after transduction with lentivirus targeting ASCT2. (h) Western blot was used to evaluated the expression of ASCT2 and Thbs1 in DOK cells after ASCT2 knockdown. (For interpretation of the references to colour in this figure legend, the reader is referred to the Web version of this article.)

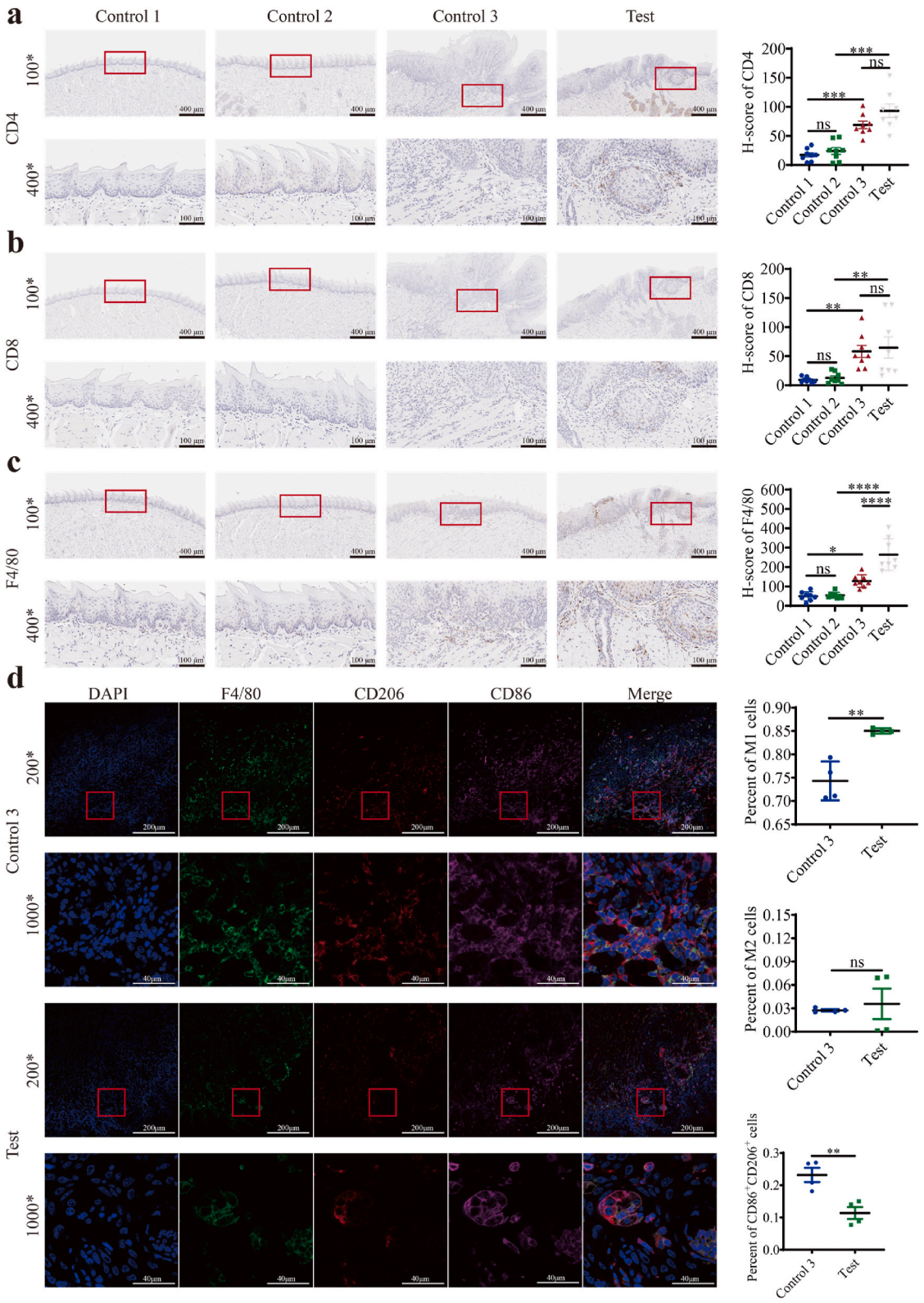

Fig. 4. ASCT2 knockout induced M1-like TAMs infiltration in cancerous sites of mice tongue treated by 4-NQO
The proportions of $CD4^+$ (a), $CD8^+$ (b) and $F4/80^+$ (c) were detected by IHC assay in four groups respectively. Left: Representative images for each group, magnification, 100* and 400*; scale bars, 400 μm for 100* magnification and 100 μm for 400* magnification. The red box showed the area of interest. Right: Quantification of CD4, CD8 and F4/80 in the four groups. (d) mIHC assay was used to evaluate the colocalization of F4/80 with CD86 or CD206 respectively in control 3 and test group. Left: Representative images for the two groups, magnification, 200* and 1000*, scale bars, 200 μm for 200* magnification and 40 μm for 1000* magnification. The red box showed the area of interest. Right: Quantification of M1 and M2 in the two groups. The above mice were all male and 8 mice for each group. (For interpretation of the references to colour in this figure legend, the reader is referred to the Web version of this article.)

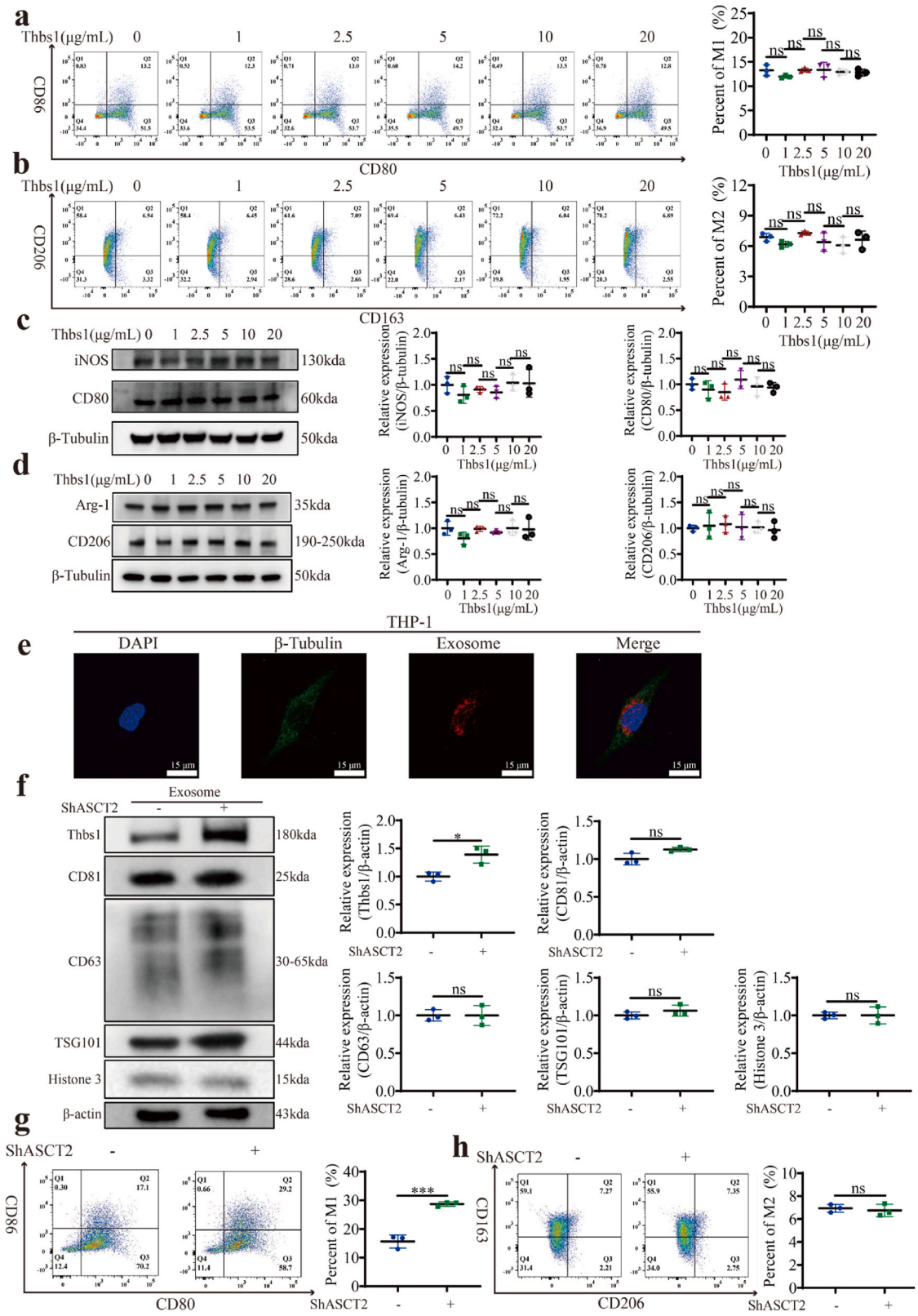

Fig. 5. Thbs1 induced the polarization of M1-like phenotype through extracellular vesicle transport pathway
THP-1 cells were treated with gradient-diluted recombinant Thbs1 protein (0, 1, 2.5, 5, 10, 20 μg/mL). (a, b) Flow cytometry was used to assess the proportion of M1-like or M2-like macrophages respectively. (c, d) Cell lysates were harvested and analyzed by Western blot for detecting M1 markers (iNOS and CD80) or M2 markers (Arg-1 and CD206). (e) Uptake of exosomes by THP-1-derived macrophages. The markers were β-Tubulin (green), exosomes (red) and nucleus (blue) respectively. Scale bar, 15 μm. (f) Thbs1 expression of exosomes from ASCT2 knockdown cells was assessed by Western blot. (g, h) Flow cytometry was used to calculate the proportion of M1-like or M2-like macrophages after treated with exosomes respectively. The above experiments were repeated 3 times. (For interpretation of the references to colour in this figure legend, the reader is referred to the Web version of this article.)

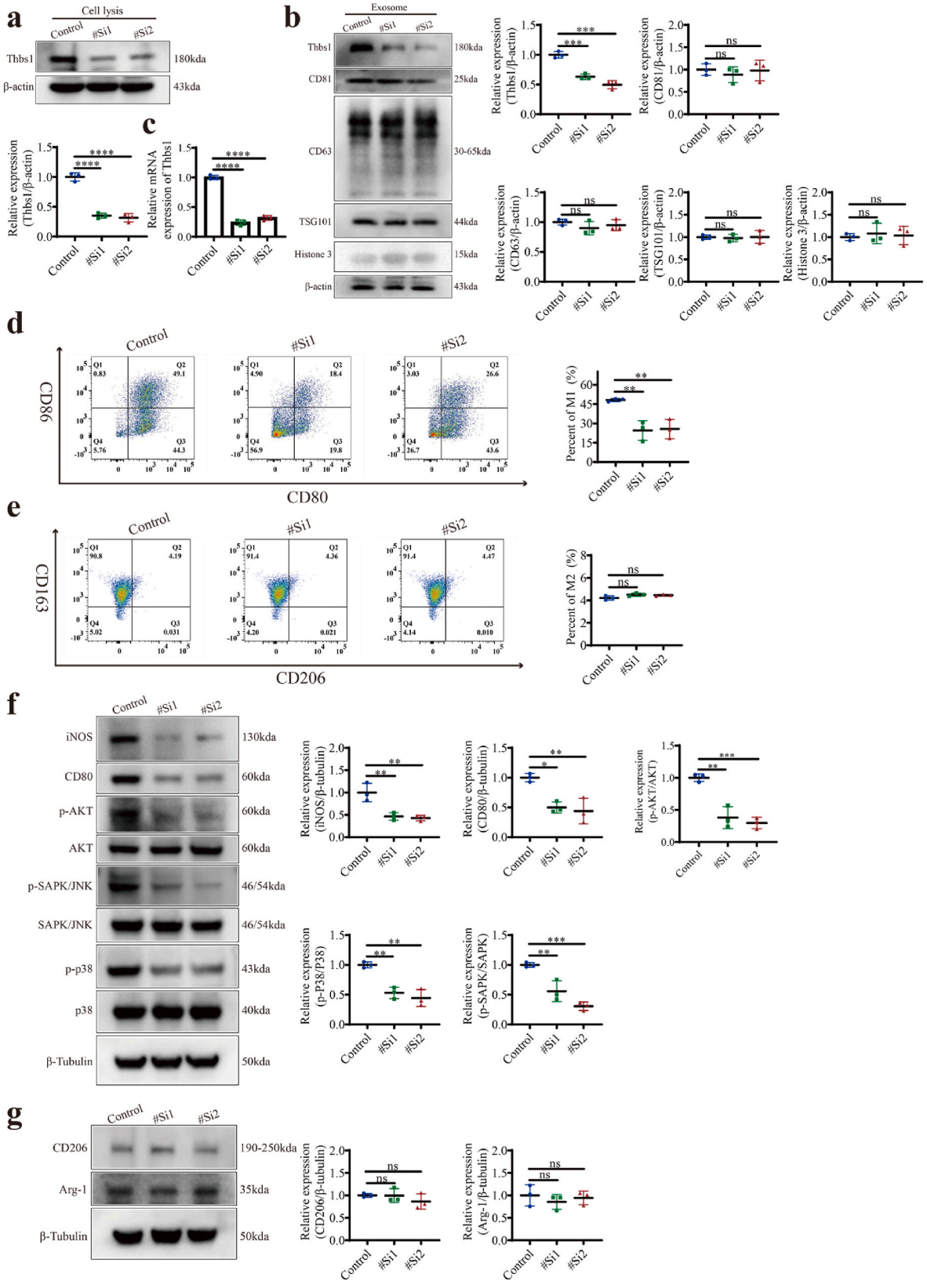

Fig. 6. Targeted Thbs1 inhibited the polarization of M1-like TAMs through p38, Akt and SAPK/JNK signaling
(a, c) Thbs1 expression was measured by Western blot and PCR assay in DOK cells transfected with siRNAs targeting Thbs1 (#Si1, #Si2) based on ASCT2 knockdown. (b) Western blot was used to detect the Thbs1 level in exosomes. (d, e) The percentage of M1-like or M2-like macrophages was analyzed by flowcytometry after treated with exosomes from Thbs1 knockdown DOK cells. (f) THP-1-derived macrophages were treated with exosomes isolated from Thbs1 knockdown cells. Cell lysates were acquired an analyzed by Western blot for detecting iNOS, CD80 and p38, Akt, SAPK/JNK signals. (g) The markers of M2-like macrophages (Arg-1 and CD206) were assessed by Western blot. The above experiments were repeated 3 times.

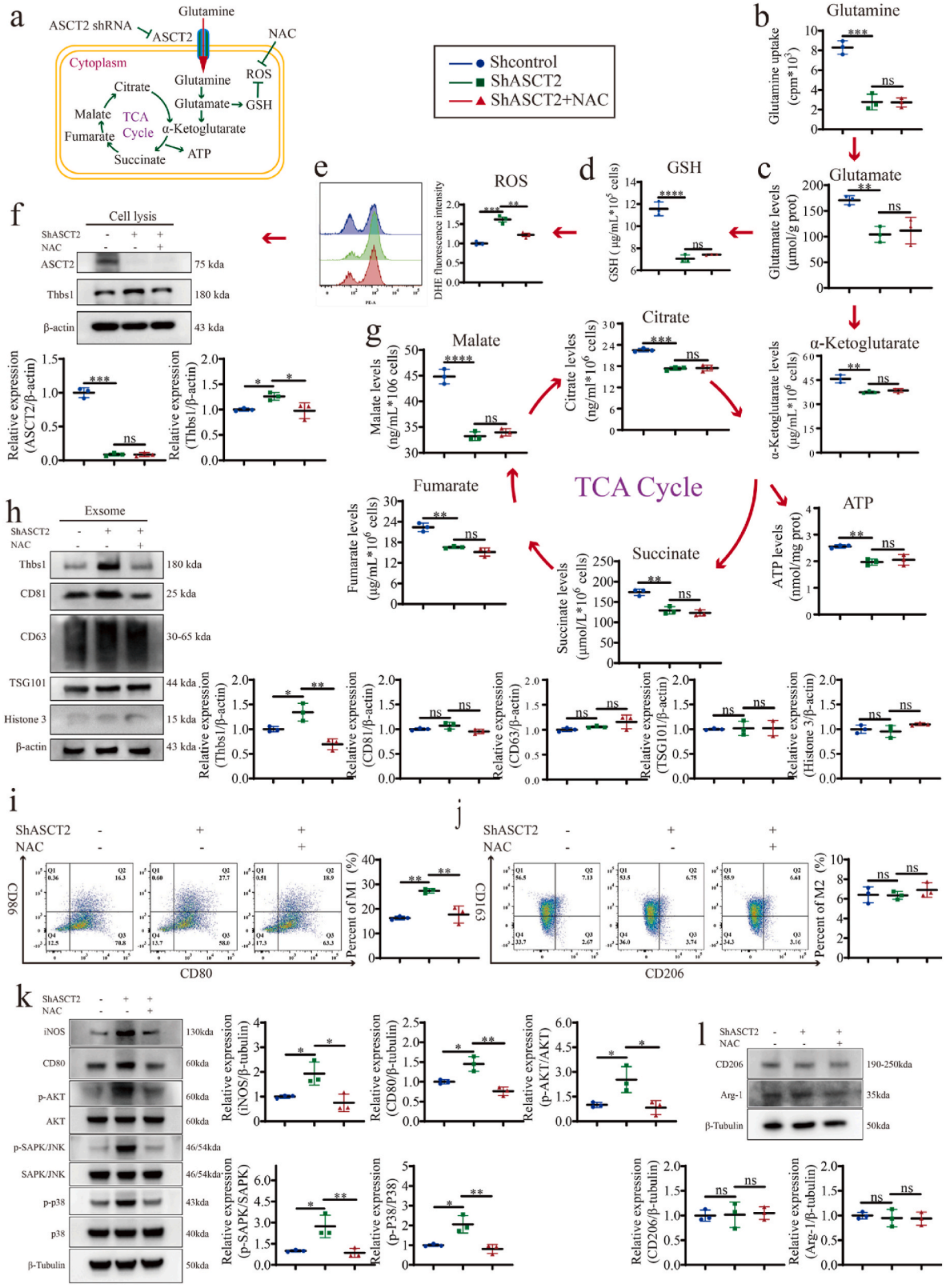

Fig. 7. ASCT2 knockdown upregulated Thbs1 expression by inducing ROS accumulation and thereby promoted M1-like TAMs polarization
(a) Schematic diagram of glutamine metabolism. (b–e) Steady-state metabolite levels of Gln, glutamate, GSH and ROS were assessed. (f, h) Thbs1 expression was detected in whole cell lysis and exosomes respectively. (g) TCA-cycle metabolites (α-KG, citrate, malate, fumarate, succinate and ATP levels) were measured using kits. (i, j) Flowcytometry was conducted to examine the M1-like and M2-like macrophages polarization respectively. (k) Western blot was used to detect iNOS, CD80 and p38, Akt, SAPK/JNK signals. (l) The markers expression of M2-like macrophages (Arg-1 and CD206) was assessed by Western blot. The above experiments were repeated 3 times. NAC, N-acetylcysteine.

3.2. Oxidative stress promoted oral carcinogenesis in ASCT2 conditional knockout mice

To examine the effects of ASCT2 knockout in oral mucosa epithelium on malignant transformation of OLK, 4-NQO was used to induce the tongue carcinogenesis mouse model. As shown in Fig. 2a, transgenic mice with the same gene background ($Slc1a5^{f/f}$ $Cre^{+/-}$) were randomly divided into 4 groups. There was no significant change in body weight of mice between control 1 and control 2 or control 3 and test, which indicated that ASCT2 knockout of oral mucosa epithelium didn't influence body weight. Actually, it was the 4-NQO treatment that decreased the body weight of mice (Fig. 2b). After exposure to 4-NQO for 16 weeks and then normal water for 4 weeks, tongue tissues of mice showed obvious epithelial hyperplasia in appearance and dysplasia in histology (Fig. 2c and d). The mean scores of lesions were significantly higher in the test group than in the control 3 group (21.88 ± 7.40 vs 13.13 ± 6.42, $P < 0.01$) (Fig. 2e). The results of pathological examination manifested that test group showed the upregulated ratio of high-grade lesion (including severe dysplasia and carcinoma) from 12.5 % to 75 % and increased counts of high-grade lesion ($P < 0.01$) compared with control 3 group (Fig. 2f–h). As shown in Fig. 2i, the PCNA H-score in test group increased from 181.9 ± 57.09 to 270.9 ± 87.13 ($P < 0.05$). Above results indicated that oxidative stress induced by ASCT2 knockout was closely associated with malignant transformation of oral cells from dysplasia to squamous cell carcinoma.

3.3. ASCT2 knockout upregulated the expression of Thbs1 in vitro and in vivo

To further explore the mechanism by which ASCT2 deletion of oral mucosa epithelium promoted OSCC, mRNA sequencing was conducted on the tongue epithelium of above four groups. We identified 33 overlapping genes through Venn diagram (Fig. 3a). Among these 33 genes, there were 25 upregulated genes and 8 downregulated genes between control 3 group and test group (Fig. 3b). We then determined Thbs1 as potential candidate which was closely linked to macrophage infiltration through GO enrichment and previous researches [34–36] (Fig. 3c and Fig. S2, Supporting information). The results of IHCassay demonstrated that 4-NQO treatment upregulated the expression of Thbs1 which was consistent with the TCGA cohort analysis, and ASCT2 knockout further enhanced Thbs1 expression (Fig. 3d, e and Fig. S2, Supporting information). In addition, the Kaplan-Meier analysis showed that the high expression of Thbs1 was correlated with poor prognosis in HNSCC (Fig. S2, Supporting information). Subsequently, we transfected lentivirus into DOK cells to generate ASCT2 knockdown cell line (Fig. 3f and g). The results of Western blot showed that ASCT2 knockdown upregulated the expression of Thbs1 (Fig. 3h). The above results suggested that targeted ASCT2 knockout promoted Thbs1 expression.

3.4. ASCT2 knockout prompted M1-like TAMs enrichment in cancerous sites of 4-NQO-treatment mice

Previous studies demonstrated that Thbs1 was associated with TAMs infiltration in tumor immune microenvironment (TME) [34–36]. In addition, our study and previous reports showed that glutamine metabolism participated in immune infiltration and was strictly related to the activation of most immune cells including lymphocytes and macrophages [13,16,37–39]. Hence, we further evaluated the infiltration of T cells and macrophages in oral mucosa after ASCT2 deletion. The results of IHC assay showed that the proportion of $CD4^+$ and $CD8^+$ T cells increased during the development of OLK, but ASCT2 deletion of oral mucosa epithelium didn't affect the enrichment of T cells (Fig. 4a and b). Similar results were also observed in neutrophils infiltration (Fig. S3, Supporting information). However, what interested us is the noticeable alteration in the proportion of macrophages. Building upon the increased percentage of macrophages induced by only 4-NQO treatment, ASCT2 knockout further enhanced macrophage infiltration (Fig. 4c). Previous studies reported that activated macrophages were classically classified into two populations, M1 and M2 [40–43]. We therefore analyzed the proportion of M1 and M2 respectively by mIHC assay. As shown in Fig. 4d, the ratio of $F4/80^+$ $CD86^+$ macrophages (M1-like TAMs) was significantly upregulated in the test group compared with control 3 group, which indicated that ASCT2 deletion may promote carcinogenesis of OLK by inducing the polarization of macrophages to M1-like TAMs.

3.5. Thbs1 promoted M1-like phenotype polarization via extracellular vesicle transport

It has been reported that Thbs1 can function by binding to receptors of cell surface like integrins and CD47 on the one hand, and enter cells by exosome delivering on the other hand [34,44–46]. Therefore, we initially treated THP-1 cells with gradient-diluted recombinant Thbs1 protein (Absin Bioscience Inc., Shanghai, China) in the process of macrophage differentiation *in vitro*. As shown in Fig. 5a–d, there was no effect on the ratio of M1-like or M2-like TAMs upon gradient-diluted recombinant Thbs1 protein treatment (0, 1, 2.5, 5, 10, 20 μg/mL), which indicated Thbs1 didn't affect the macrophage polarization by binding to cell surface receptors.

Afterwards, we managed to isolate exosomes from conditioned medium (CM). TEM results showed the bilayer membranous "cup-concave" morphology of exosome (Fig. S4a, Supporting information). NanoFCM demonstrated that the size of extracted vesicles is 40–120 nm which is the common diameter range for exosome (Fig. S4b, Supporting information). Western blot analysis further confirmed the positive expression of exosome markers (CD81, CD63 and TSG101) and the negative expression of nuclear protein marker (Histone 3) (Fig. S4c, Supporting information). As shown in Fig. 5e, we observed the uptake of fluorescence-labeled exosomes by THP-1-derived macrophages, indicating macrophages could obtain the biological signals from exosome by direct uptake.

We next examined the Thbs1 expression in exosomes. The results of Western blot showed that ASCT2 knockdown upregulated the expression of Thbs1 in exosomes (Fig. 5f). Afterwards, equal amount of exosome supernatant was used to stimulate macrophages. Comparatively, exosomes from ASCT2 knockdown DOK cells played critical roles in promoting M1-like macrophages polarization (Fig. 5g and h). In addition, Dynasore (Selleck, Co., Ltd, Shanghai, China), an inhibitor of the endocytosis pathway, could restrain the polarization of M1-like macrophages by inhibiting the exosome uptake (Fig. S5, Supporting information). On the basis of ASCT2 knockdown, targeted interference with Thbs1 expression in exosome by siRNA could significantly inhibit the polarization of M1-like macrophages through blocking p38, Akt and SAPK/JNK signaling which was in line with previous studies [47], while didn't affect the proportion of M2-like macrophages (Fig. 6a–g).

3.6. ASCT2 knockdown promoted Thbs1 expression and M1-like TAMs polarization through inducing oxidative stress

As previously shown, ASCT2 deletion promoted the ROS production of oral mucosa epithelium, especially after 4-NQO treatment, and induced the carcinogenesis of OLK *in vivo*. Hence, we hypothesized that the accumulation of intracellular ROS leaded to the upregulation of Thbs1. As the established role of ASCT2 in Gln metabolism, we examined the corresponding metabolites under ASCT2 knockdown or N-acetylcysteine (NAC, sigma-Aldrich, St. Louis, MO, USA) treatment. ASCT2 knockdown decreased the intracellular Gln level (Fig. S6a and b, Supporting information), while NAC, a precursor of GSH, didn't affect Gln uptake (Fig. 7a and b). Glutamate and GSH levels were also remarkably decreased by ASCT2 knockdown (Fig. 7c, d, Fig. S6c and d, Supporting information). Consistently, targeted interference ASCT2-mediated Gln uptake upregulated ROS level, but NACinhibit the

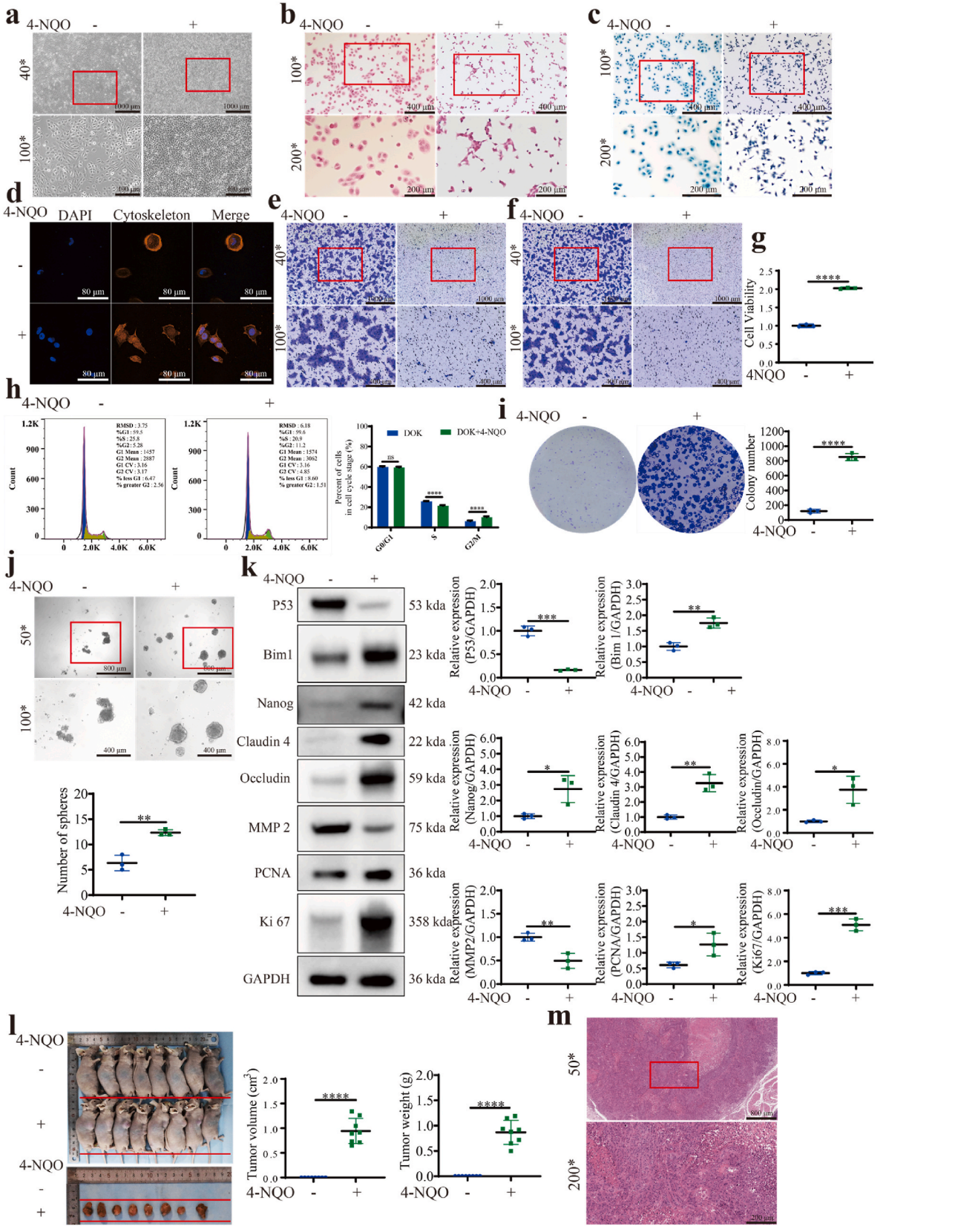

(caption on next page)

Fig. 8. 4-NQO treatment significantly increased carcinogenecitty of DOK cells
(a) Cell growth status was acquired by inverted contrasting microscope, magnification, 40* and 100*, scale bars, 1000 μm for 40* magnification and 400 μm for 100* magnification. The red box showed the area of interest. HE (b) and Papanicolaou staining (c) were used to observe cell morphology, magnification, 100* and 200*, scale bars, 400 μm for 100* magnification and 200 μm for 200* magnification. The red box showed the area of interest. (d) Cytoskeleton staining was performed to assess cytoskeleton between DOK and DOK-4-NQO cells, scale bars, 80 μm. Cell migration (e) and cell invasion assay (f) were conducted to detect the abilities of cell migration and invasion, magnification, 40* and 100*, scale bars, 1000 μm for 40* magnification and 400 μm for 100* magnification. The red box showed the area of interest. CCK-8 assay (g), cell cycle assay (h), and colony formation assay (i) were used to evaluate the proliferation ability between DOK and DOK-4-NQO cells. (j) Tumor sphere formation assay was conducted to assess the stemness, magnification, 50* and 100*, scale bars, 800 μm for 50* magnification and 400 μm for 100* magnification. The red box showed the area of interest. (k) Western blot was performed to examine the expression of p53, Bim1, Nanog, Claudin 4, Occluding, MMP2, Ki 67, PCNA between DOK and DOK-4-NQO cells. (l) Xenograft experiment (male nude mice) was used to compare the tumorgenicity. Left: Representative images of xenograft tumors. Right: Tumor Volume and weight of xenografts in the ending point respectively, Tumor volume=(length × width^2)/2. (m) Representative HE images of xenograft tumors. magnification, 50* and 200*; scale bars, 800 μm for 50* magnification and 200 μm for 200* magnification. The red box showed the area of interest. The above experiments were repeated 3 times. (For interpretation of the references to colour in this figure legend, the reader is referred to the Web version of this article.)

production of ROS (Fig. 7e and Fig. S6e, Supporting information). As shown in Fig. 7f and h, ASCT2 knockdown elevated Thbs1 expression, while NAC inhibited the expression of Thbs1 whether in cells or exosome. Subsequently, we demonstrated that ASCT2 knockdown significantly decreased intracellular α-KG, citrate, malate, fumarate and succinate levels (metabolites in TCAcycle), attended by reduced ATP, but NACtreatment had no effect (Fig. 7g and Fig. S6f, Supporting information).

Macrophage differentiation assay *in vitro* showed that M1-like macrophages polarization was obviously inhibited by exosomes derived from DOK cells treated by NAC (Fig. 7i and k), but M2-like macrophages polarization wasn't affected (Fig. 7j and l). In addition, exosomes of DOK cells based on ASCT2 knockdown triggered M1-like macrophages polarization through activating p38, Akt and SAPK/JNK signaling. However, exosomes produced by DOK after NAC treatment had the opposite effect which was in consistent with the interference of Thbs1 by siRNA (Fig. 7k). Altogether, these results suggested that targeted interference ASCT2-mediated Gln uptake contributed to ROS accumulation, which in turn upregulated Thbs1 expression in exosome, thereby polarizing macrophages to an M1-like phenotype.

3.7. DOK cells showed significantly increased carcinogenicity treated with 4-NQO

To investigate the biological functions of 4-NQO on DOK cells, we firstly treated DOK cells with 2.6 μM 4-NQO for 2 months intermittently to generate the transformed cell line DOK-4-NQO *in vitro*. Subsequently, we evaluated cell morphology, proliferation ability, migration and invasion ability, colony formation and tumorgenicity. As shown in Fig. 8a, DOK cells presented noticeably contact inhibition, but DOK-4-NQO cells displayed uncontrolled cell division with overlapping. Furthermore, DOK-4-NQO cells showed the increased ratio of nucleus to plasma, more cell division and sporadic tumor giant cells (Fig. 8b and c). Notably, we observed cytoskeleton remodeling of DOK-4-NQO cells exhibiting fewer and longer filopodia (Fig. 8d). Not surprisingly, the migration and invasion ability of DOK-4-NQO cells were significantly inhibited (Fig. 8e and f). The results of cell cycle assay, CCK-8 and colony formation assay demonstrated increased proliferation ability of Dok-4-NQO cells (Fig. 8g–i). Microsphere forming assay revealed that the tumor formation capacity was significantly elevated in DOK-4-NQO cells (Fig. 8j). Western blot further confirmed that DOK-4-NQO cells showed increased proliferation ability, enhanced stemness, intensive cell connections and decreased cell invasion (Fig. 8k). Additionally, the expression of tumor suppressor p53 was significantly reduced in DOK-4-NQO cells (Fig. 8k). In addition, the results of xenograft experiments *in vivo* showed that none of nude mice subcutaneously injected with DOK cells developed tumors, while the tumorigenesis ratio of DOK-4-NQO cells was 100 % (Fig. 8l). HE staining also manifested that tumors were typical squamous cell carcinoma (Fig. 8m). All these results demonstrated that 4-NQO promoted the carcinogenicity of DOK cells.

3.8. CM from M1-like TAMs promoted the tumorgenicity of DOK-4-NQO cells

Aiming to explore whether CM from M1-like TAMs can promote carcinogenesis, CM from M0 or M1-like TAMs was harvested to treat DOK-4-NQO cells respectively. Comparatively, CM from M1-like TAMS significantly increased proliferation ability (Fig. 9a and b). CM from M1-like TAMS also increased colony formation ability (Fig. 9c). Moreover, CM from M1-like TAMS contributed to a dramatic elevation in cell migration and invasion abilities (Fig. 9d and e). Microsphere forming assay suggested that tumor formation capacity was significantly elevated under the treatment of CM from M1-like TAMS (Fig. 9f). The results of Western blot further determined that CM from M1-like TAMS upregulated the expression of proliferation marker (PCNA), stemness markers (Bim 1 and Nanog) and invasion marker (MMP2), but decreased the level of claudin 4 and occluding (Fig. 9g). Besides, the tumor forming of xenografts was greatly increased under the treatment of CM from M1-like TAMS (Fig. 9h). The results of IHC further showed that CM from M1-like TAMS enhanced the levels of PCNA and Bim 1, while downregulated Occludin level of xenografts (Fig. 9i). The above results demonstrated that M1-like TAMS aggravated malignant behaviors of DOK-4-NQO cells.

4. Discussion

ROS plays critical homeostatic roles, while oxidative stress is both a cause and a consequence of multiple diseases including OSCC [29,48]. *In vitro* studies showed that Gln metabolism participates in the synthesis of GSH to protect cells from oxidative stress [15–17,32,33]. However, it remains unclear whether targeted interference with ASCT2-mediated Gln uptake *in vivo* contributes to oxidative stress and further promotes OSCC progression. In current study, we initially constructed transgenic mice where ASCT2 was specifically deleted in oral mucosa epithelium. we found that ASCT2 deletion *in vivo* leaded to oxidative stress, and promoted carcinogenesis of OLK under 4-NQO treatment. Furthermore, ROS caused by targeted ASCT2 effectively upregulated Thbs1 expression in exosome, which polarized macrophages to an M1-like phenotype and thereby advanced malignant progression of OSCC (Fig. 10). To our best knowledge, these results firstly identified that oxidative stress triggered by ASCT2 knockout promoted oral carcinogenesis, which strongly suggested that maintaining redox homeostasis possibly served as a preventative and therapeutic strategy in the initial stage of tumors.

Oxidative stress can occur from increased ROS production including H_2O_2, ·OH and $ONOO^-$, or from decreased antioxidant like GSH, which can cause oxidative damage to lipid, protein and nucleic acids. In consistent with the standard of oxidative stress detection, our research found that ASCT2 deletion of oral mucosa epithelium *in vivo* significantly downregulated GSH level and promoted ROS accumulation which caused the upregulation of DNA damage markers including 8-OHdG and γ-H2AX. Previous studies reported that targeted ASCT2-mediated Gln uptake induced excessive production of ROS *in vitro* [16,

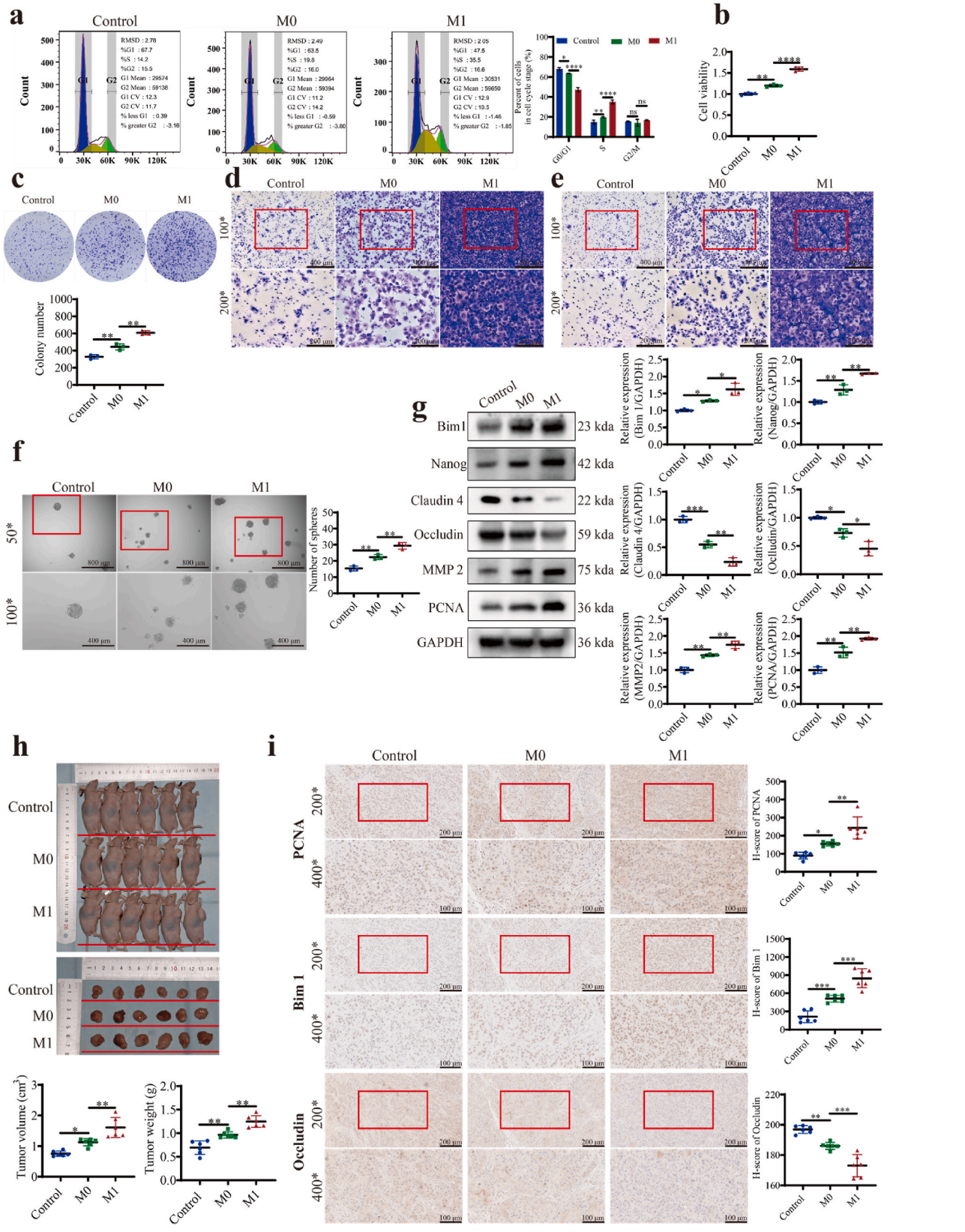

(caption on next page)

Fig. 9. DOK-4-NQO cells showed increased tumorgenicity treated with CM from M1-like TAMs
Cell cycle assay (a) and CCK-8 assay(b) were used to detect proliferation ability of CM on DOK-4-NQO cells. The effect of CM on the colony formation was evaluated by colony formation assay(c). The abilities of migration (d) invasion (e) were determined by, cell migration and cell invasion assay. magnification, 100* and 200*, scale bars, 400 μm for 100* magnification and 200 μm for 200* magnification. The red box showed the area of interest. (f) Tumor sphere formation assay was conducted to assess the stemness, magnification, scale bars, 800 μm for 50* magnification and 400 μm for 100* magnification. The red box showed the area of interest. (g) Western blot was conducted to further assess stemness (Bim1 and Nanog), cell junction (Claudin 4 and Occludin), invasion (MMP2) and proliferation (PCNA) of CM on DOK-4-NQO cells. (h) Xenograft experiment (male nude mice) was used to evaluate the tumorgenicity of CM on DOK-4-NQO cells. Upper: Representative images of xenograft tumors. Lower: Tumor Volume and weight of xenografts in the ending point respectively, Tumor volume=(length × width^2)/2. (i) The levels of PCNA, Bim 1 and Occludin in xenograft tumors were assessed by IHC, magnification, 200* and 400*, scale bars, 200 μm for 200* magnification and 100 μm for 400* magnification. The red box showed the area of interest. The above experiments were repeated 3 times. (For interpretation of the references to colour in this figure legend, the reader is referred to the Web version of this article.)

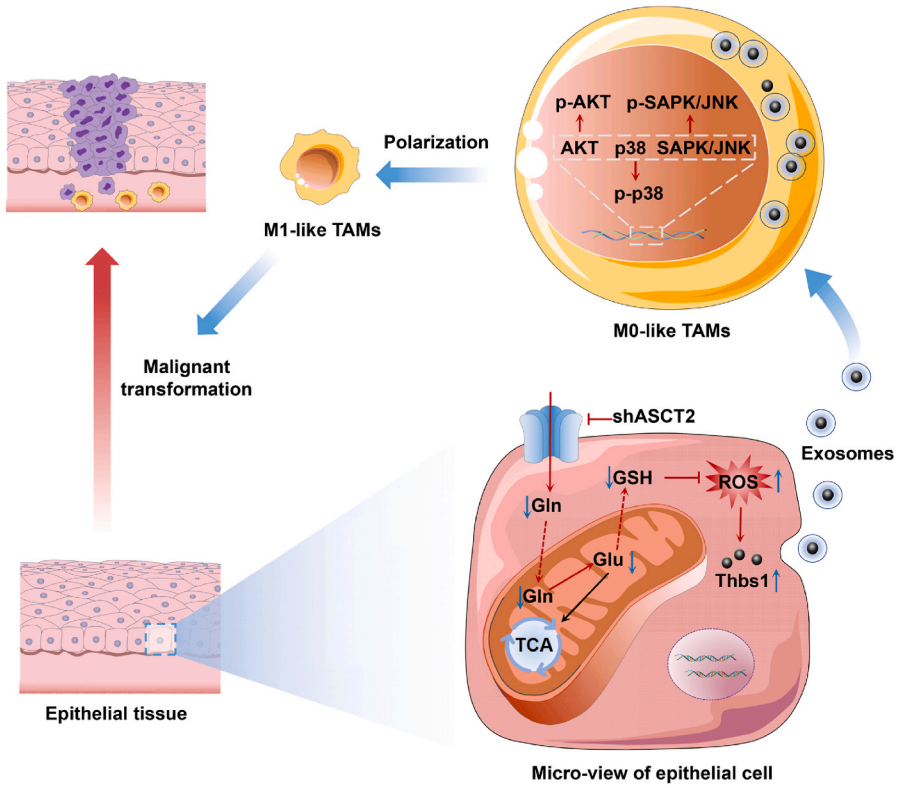

Fig. 10. Model diagram for the role of ROS in M1-like TAMs-mediated oral carcinogenesis by exosome-transferring Thbs1
In oral keratocytes, targeted interference with ASCT2-mediated Gln uptake inhibits the synthesis of GSH and thereby induces the accumulation of ROS, which in turn upregulates Thbs1 expression. Thbs1 then activates p38, Akt and SAPK/JNK signaling to polarize M1-like TAMs by exosome-transferred pathway, which finally promotes oral carcinogenesis.

49–51], while we firstly found that ASCT2 knockout induced oxidative stress *in vivo*.

Throughout of the development and progression of OSCC, the TME and its crosstalk with the tumor are of great importance. It has been reported that tumor cells can directly affect immune cells infiltration including TAMs [52]. For example, previous studies showed that β-defensin 3 or lactate in OLK and OSCC could induce TAMs infiltration and promote M2-like TAMs polarization [53–55]. Additionally, it has been recently reported that M1-like TAMs could activate epithelial-to-mesenchymal transition (EMT), thereby speeding up invasion and metastasis of OSCC [24,56]. To further understand the genetic changes during the carcinogenesis of the mice model, we determined Thbs1 as potential candidate regulator by mRNA sequencing and found that Thbs1 was closely associated with the enrichment of TAMs. In addition, we found there was a more significant increase of M1-like TAMs in the cancerous area, which indicated that Thbs1 may promote the infiltration of M1-like TAMs in the oral carcinogenesis of ASCT2 knockout mice.

Thbs1 is a multifunction secreted proteins with powerful pro-inflammatory and pro-migratory effects on macrophages [57]. It can function by engaging receptors of cell surface including integrins and CD47 on the one hand, or regulate intercellular signaling by exosome on the other hand [34,44–46]. Our data showed that gradient-diluted recombinant Thbs1 protein treatment didn't affect M1-like polarization, while exosome from ASCT2 knockdown cells absolutely promoted M1-like phenotype, which demonstrated that Thbs1 polarized M1-like TAMs by exosome-transferred pathway. Moreover, our study further demonstrated that Thbs1 in exosomes triggered M1-like TAMs polarization by activating p38, Akt and SAPK/JNK signaling, which was in line with previous report [47].

ASCT2-mediated Gln uptake is not only involved in the TCA cycle to ensure the energy supply, but also participates in GSH synthesis to sustain redox hemostasis [58,59]. It has been reported that targeted interference with ASCT2 can inhibit cell proliferation and induce ROS production [17,27,60]. ROS, serving as a critical signaling molecule, plays an important role in supporting cell behavior by regulating the expression of genes related to cell proliferation, cell survival and differentiation, including NF-κB and NRF2 [2,61]. Therefore, we

speculated that the upregulation of Thbs1 was attributed to ROS accumulation caused by ASCT2 knockdown. In consistent with our hypothesis, we demonstrated that targeted ASCT2 increased ROS level by inhibiting the synthesis of GSH to promote the expression of Thbs1.

It's reported that high infiltration of M1-like TAMs is associated with malignant features in some tumors [62–64]. In this study, we found that TAMs, especially M1-like TAMs, were less in normal oral mucosa and OLK compared with OSCC, which indicated that M1-like TAMs may be essential during the carcinogenesis and progression of OSCC. To further verify the roles of M1-like TAMs, we generated a DOK transformed cell line using 4-NQO and treated it with CM from M0 or M1-like TAMs. Not surprisingly, M1-like TAMs promoted the progression of OSCC both in *vitro* and *in vivo*. Our study firstly confirmed that M1-like TAMs played a pivotal role in oral carcinogenesis evoked by oxidative stress.

In summary, targeted interference with ASCT2-mediated Gln uptake contributed to ROS accumulation, and thereby activated M1-like TAMs by exosome-transferred Thbs1 to promote malignant progression of OSCC, and alleviating oxidative stress shows great potentials for prevent oral carcinogenesis.

Funding

This work was supported by grants from the National Natural Science Foundation of China (82270975, 81771070).

CRediT authorship contribution statement

Wei Li: Writing – original draft, Methodology, Investigation, Formal analysis. **Qingwen Zeng:** Validation, Investigation. **Bing Wang:** Validation, Formal analysis. **Chao Lv:** Investigation. **Haoan He:** Formal analysis. **Xi Yang:** Writing – review & editing, Conceptualization. **Bin Cheng:** Writing – review & editing, Data curation, Conceptualization. **Xiaoan Tao:** Writing – review & editing, Supervision, Funding acquisition, Data curation, Conceptualization.

Declaration of competing interest

The authors declare the following financial interests/personal relationships which may be considered as potential competing interests: Xiaoan Tao reports was provided by National Natural Science Foundation of China. If there are other authors, they declare that they have no known competing financial interests or personal relationships that could have appeared to influence the work reported in this paper.

Data availability

Data will be made available on request.

Appendix A. Supplementary data

Supplementary data to this article can be found online at https://doi.org/10.1016/j.redox.2024.103335.

References

[1] H. Sies, D.P. Jones, Reactive oxygen species (ROS) as pleiotropic physiological signalling agents, Nat. Rev. Mol. Cell Biol. 21 (7) (2020) 363–383, https://doi.org/10.1038/s41580-020-0230-3.
[2] E.C. Cheung, K.H. Vousden, The role of ROS in tumour development and progression, Nat. Rev. Cancer 22 (5) (2022) 280–297, https://doi.org/10.1038/s41568-021-00435-0.
[3] C.-F. Mo, J. Li, S.-X. Yang, et al., IQGAP1 promotes anoikis resistance and metastasis through Rac1-dependent ROS accumulation and activation of Src/FAK signalling in hepatocellular carcinoma, Br. J. Cancer 123 (7) (2020) 1154–1163, https://doi.org/10.1038/s41416-020-0970-z.
[4] H. Chang, J. Li, K. Qu, et al., CRIF1 overexpression facilitates tumor growth and metastasis through inducing ROS/NFκB pathway in hepatocellular carcinoma, Cell Death Dis. 11 (5) (2020) 332, https://doi.org/10.1038/s41419-020-2528-7.
[5] Y. Wang, H. Qi, Y. Liu, et al., The double-edged roles of ROS in cancer prevention and therapy, Theranostics 11 (10) (2021) 4839–4857, https://doi.org/10.7150/thno.56747.
[6] H.C. Yoo, Y.C. Yu, Y. Sung, et al., Glutamine reliance in cell metabolism, Exp. Mol. Med. 52 (9) (2020) 1496–1516, https://doi.org/10.1038/s12276-020-00504-8.
[7] H.T. Lee, C.S. Lin, S.C. Pan, et al., Alterations of oxygen consumption and extracellular acidification rates by glutamine in PBMCs of SLE patients, Mitochondrion 44 (2019) 65–74, https://doi.org/10.1016/j.mito.2018.01.002.
[8] Y. Miao, Y. Zheng, Y. Geng, et al., The role of GLS1-mediated glutaminolysis/2-HG/H3K4me3 and GSH/ROS signals in Th17 responses counteracted by PPARγ agonists, Theranostics 11 (9) (2021) 4531–4548, https://doi.org/10.7150/thno.54803.
[9] X. Yao, W. Li, D. Fang, et al., Emerging roles of energy metabolism in ferroptosis regulation of tumor cells, Adv. Sci. 8 (22) (2021) e2100997, https://doi.org/10.1002/advs.202100997.
[10] Q. Zhou, W. Lin, C. Wang, et al., Neddylation inhibition induces glutamine uptake and metabolism by targeting CRL3SPOP E3 ligase in cancer cells, Nat. Commun. 13 (1) (2022) 3034, https://doi.org/10.1038/s41467-022-30559-2.
[11] F. Ni, W.-M. Yu, Z. Li, et al., Critical role of ASCT2-mediated amino acid metabolism in promoting leukaemia development and progression, Nat. Metab. 1 (3) (2019) 390–403, https://doi.org/10.1038/s42255-019-0039-6.
[12] H. Jiang, N. Zhang, T. Tang, et al., Target the human alanine/serine/cysteine transporter 2(ASCT2): achievement and future for novel cancer therapy, Pharmacol. Res. 158 (2020) 104844, https://doi.org/10.1016/j.phrs.2020.104844.
[13] W. Song, D. Li, L. Tao, et al., Solute carrier transporters: the metabolic gatekeepers of immune cells, Acta Pharm. Sin. B 10 (1) (2020) 61–78, https://doi.org/10.1016/j.apsb.2019.12.006.
[14] H. Jin, S. Wang, E.A. Zaal, et al., A powerful drug combination strategy targeting glutamine addiction for the treatment of human liver cancer, Elife 9 (2020) e56749, https://doi.org/10.7554/eLife.56749.
[15] S. Okazaki, K. Umene, J. Yamasaki, et al., Glutaminolysis-related genes determine sensitivity to xCT-targeted therapy in head and neck squamous cell carcinoma, Cancer Sci. 110 (11) (2019) 3453–3463, https://doi.org/10.1111/cas.14182.
[16] W. Li, Z. Ling, J. Wang, et al., ASCT2-mediated glutamine uptake promotes Th1 differentiation via ROS-EGR1-PAC1 pathway in oral lichen planus, Biochem. Pharmacol. 216 (2023) 115767, https://doi.org/10.1016/j.bcp.2023.115767.
[17] Y. Luo, W. Li, Z. Ling, et al., ASCT2 overexpression is associated with poor survival of OSCC patients and ASCT2 knockdown inhibited growth of glutamine-addicted OSCC cells, Cancer Med. 9 (10) (2020) 3489–3499, https://doi.org/10.1002/cam4.2965.
[18] Z. Zhang, R. Liu, Y. Shuai, et al., ASCT2 (SLC1A5)-dependent glutamine uptake is involved in the progression of head and neck squamous cell carcinoma, Br. J. Cancer 122 (1) (2020) 82–93, https://doi.org/10.1038/s41416-019-0637-9.
[19] H. Sung, J. Ferlay, R.L. Siegel, et al., Global cancer statistics 2020: GLOBOCAN estimates of incidence and mortality worldwide for 36 cancers in 185 countries, CA Cancer J Clin 71 (3) (2021) 209–249, https://doi.org/10.3322/caac.21660.
[20] A. Romano, D. Di Stasio, M. Petruzzi, et al., Noninvasive imaging methods to improve the diagnosis of oral carcinoma and its precursors: state of the art and proposal of a three-step diagnostic process, Cancers 13 (12) (2021) 2864, https://doi.org/10.3390/cancers13122864.
[21] L. Lin, C. Song, Z. Wei, et al., Multifunctional photodynamic/photothermal nanoagents for the treatment of oral leukoplakia, J. Nanobiotechnol. 20 (1) (2022) 106, https://doi.org/10.1186/s12951-022-01310-2.
[22] S. Shen, Z. Yan, J. Wu, et al., Characterization of ROS metabolic equilibrium reclassifies pan-cancer samples and guides pathway targeting therapy, Front. Oncol. 10 (2020) 581197, https://doi.org/10.3389/fonc.2020.581197.
[23] A.D. Raddatz, C.M. Furdui, E.A. Bey, et al., Single-cell kinetic modeling of β-lapachone metabolism in head and neck squamous cell carcinoma, Antioxidants 12 (3) (2023) 741, https://doi.org/10.3390/antiox12030741.
[24] J. Bouaoud, J.-P. Foy, A. Tortereau, et al., Early changes in the immune microenvironment of oral potentially malignant disorders reveal an unexpected association of M2 macrophages with oral cancer free survival, OncoImmunology 10 (1) (2021) 1944554, https://doi.org/10.1080/2162402X.2021.1944554.
[25] J. Bouaoud, G. De Souza, C. Darido, et al., The 4-NQO mouse model: an update on a well-established in vivo model of oral carcinogenesis, Methods Cell Biol. 163 (2021) 197–229, https://doi.org/10.1016/bs.mcb.2020.09.004.
[26] G.R. Thomas, Z. Chen, M.N. Oechsli, et al., Decreased expression of CD80 is a marker for increased tumorigenicity in a new murine model of oral squamous-cell carcinoma, Int. J. Cancer 82 (3) (1999) 377–384.
[27] W. Li, Z. Ling, J. Wang, et al., ASCT2-mediated glutamine uptake promotes Th1 differentiation via ROS-EGR1-PAC1 pathway in oral lichen planus, Biochem. Pharmacol. 216 (2023) 115767, https://doi.org/10.1016/j.bcp.2023.115767.
[28] X. Zhang, Y. Jiang, J. Mao, et al., Hydroxytyrosol prevents periodontitis-induced bone loss by regulating mitochondrial function and mitogen-activated protein kinase signaling of bone cells, Free Radic. Biol. Med. 176 (2021) 298–311, https://doi.org/10.1016/j.freeradbiomed.2021.09.027.
[29] C. Ninfali, M. Cortés, M.C. Martínez-Campanario, et al., The adaptive antioxidant response during fasting-induced muscle atrophy is oppositely regulated by ZEB1 and ZEB2, Proc Natl Acad Sci U S A 120 (46) (2023) e2301120120, https://doi.org/10.1073/pnas.2301120120.
[30] S. Hänzelmann, R. Castelo, J. Guinney, GSVA: gene set variation analysis for microarray and RNA-seq data, BMC Bioinf. 14 (2013) 7, https://doi.org/10.1186/1471-2105-14-7.

[31] G. Bindea, B. Mlecnik, M. Tosolini, et al., Spatiotemporal dynamics of intratumoral immune cells reveal the immune landscape in human cancer, Immunity 39 (4) (2013) 782–795, https://doi.org/10.1016/j.immuni.2013.10.003.
[32] Y. Liu, T. Zhao, Z. Li, et al., The role of ASCT2 in cancer: a review, Eur. J. Pharmacol. 837 (2018) 81–87, https://doi.org/10.1016/j.ejphar.2018.07.007.
[33] G. Lian, J.R. Gnanaprakasam, T. Wang, et al., Glutathione de novo synthesis but not recycling process coordinates with glutamine catabolism to control redox homeostasis and directs murine T cell differentiation, Elife 7 (2018) e36158, https://doi.org/10.7554/eLife.36158.
[34] E.V. Stein, T.W. Miller, K. Ivins-O'Keefe, et al., Secreted thrombospondin-1 regulates macrophage interleukin-1β production and activation through CD47, Sci. Rep. 6 (2016) 19684, https://doi.org/10.1038/srep19684.
[35] A. Kale, N.M. Rogers, K. Ghimire, Thrombospondin-1 CD47 signalling: from mechanisms to medicine, Int. J. Mol. Sci. 22 (8) (2021) 4062, https://doi.org/10.3390/ijms22084062.
[36] S. Kaur, S.M. Bronson, D. Pal-Nath, et al., Functions of thrombospondin-1 in the tumor microenvironment, Int. J. Mol. Sci. 22 (9) (2021) 4570, https://doi.org/10.3390/ijms22094570.
[37] R.D. Leone, L. Zhao, J.M. Englert, et al., Glutamine blockade induces divergent metabolic programs to overcome tumor immune evasion, Science 366 (6468) (2019) 1013–1021, https://doi.org/10.1126/science.aav2588.
[38] K. Kashfi, J. Kannikal, N. N, Macrophage reprogramming and cancer therapeutics role of iNOS-derived NO, Cells 10 (11) (2021) 3194, https://doi.org/10.3390/cells10113194.
[39] P.-S. Liu, Y.-T. Chen, X. Li, et al., CD40 signal rewires fatty acid and glutamine metabolism for stimulating macrophage anti-tumorigenic functions, Nat. Immunol. 24 (3) (2023) 452–462, https://doi.org/10.1038/s41590-023-01430-3.
[40] P.J. Murray, J.E. Allen, S.K. Biswas, et al., Macrophage activation and polarization: nomenclature and experimental guidelines, Immunity 41 (1) (2014) 14–20, https://doi.org/10.1016/j.immuni.2014.06.008.
[41] H. Xu, J. Zhu, S. Smith, et al., Notch-RBP-J signaling regulates the transcription factor IRF8 to promote inflammatory macrophage polarization, Nat. Immunol. 13 (7) (2012) 642–650, https://doi.org/10.1038/ni.2304.
[42] P. Italiani, D. Boraschi, From monocytes to M1/M2 macrophages: phenotypical vs. Functional differentiation, Front. Immunol. 5 (2014) 514, https://doi.org/10.3389/fimmu.2014.00514.
[43] Shanze Chen, Abdullah F.U. H. Saeed, Quan Liu, et al., Macrophages in immunoregulation and therapeutics, Signal Transduct Target Ther 8 (1) (2023) 207, https://doi.org/10.1038/s41392-023-01452-1.
[44] S. Patwardhan, P. Mahadik, O. Shetty, et al., ECM stiffness-tuned exosomes drive breast cancer motility through thrombospondin-1, Biomaterials 279 (2021) 121185, https://doi.org/10.1016/j.biomaterials.2021.121185.
[45] J. Li, H. Feng, J. Zhu, et al., Gastric cancer derived exosomal THBS1 enhanced Vγ9Vδ2 T-cell function through activating RIG-I-like receptor signaling pathway in a N6-methyladenosine methylation dependent manner, Cancer Lett. 576 (2023) 216410, https://doi.org/10.1016/j.canlet.2023.216410.
[46] M.S.U. Ahmed, B.D. Lord, Addai B. Adu, et al., Immune profile of exosomes in african American breast cancer patients is mediated by kaiso/THBS1/CD47 signaling, Cancers 15 (8) (2023) 2282, https://doi.org/10.3390/cancers15082282.
[47] M. Xiao, J.J. Zhang, W.J. Chen, et al., M1-like tumor-associated macrophages activated by exosome-transferred THBS1 promote malignant migration in oral squamous cell carcinoma, J. Exp. Clin. Cancer Res. 37 (2018) 143, https://doi.org/10.1186/s13046-018-0815-2.
[48] A. Cuadrado, A.I. Rojo, G. Wells, et al., Therapeutic targeting of the NRF2 and KEAP1 partnership in chronic diseases, Nat. Rev. Drug Discov. 18 (4) (2019) 295–317, https://doi.org/10.1038/s41573-018-0008-x.
[49] D.R. Wise, R.J. DeBerardinis, A. Mancuso, et al., Myc regulates a transcriptional program that stimulates mitochondrial glutaminolysis and leads to glutamine addiction, Proc Natl Acad Sci U S A 105 (48) (2008) 18782–18787, https://doi.org/10.1073/pnas.0810199105.
[50] B.J. Altman, Z.E. Stine, C.V. Dang, From Krebs to clinic: glutamine metabolism to cancer therapy, Nat. Rev. Cancer 16 (10) (2016) 619–634, https://doi.org/10.1038/nrc.2016.71.
[51] H.-N. Kung, J.R. Marks, J.-T. Chi, Glutamine synthetase is a genetic determinant of cell type-specific glutamine independence in breast epithelia, PLoS Genet. 7 (8) (2011) e1002229, https://doi.org/10.1371/journal.pgen.1002229.
[52] G. Ma, Y. Liang, Y. Chen, et al., Glutamine deprivation induces PD-L1 expression via activation of EGFR/ERK/c-Jun signaling in renal cancer, Mol. Cancer Res. : MCR 18 (2) (2020) 324–339, https://doi.org/10.1158/1541-7786.MCR-19-0517.
[53] R. Rangel, C.R. Pickering, A.G. Sikora, et al., Genetic changes driving immunosuppressive microenvironments in oral premalignancy, Front. Immunol. 13 (2022) 840923, https://doi.org/10.3389/fimmu.2022.840923.
[54] H.I. Kawsar, A. Weinberg, S.A. Hirsch, et al., Overexpression of human beta-defensin-3 in oral dysplasia: potential role in macrophage trafficking, Oral Oncol. 45 (8) (2009) 696–702, https://doi.org/10.1016/j.oraloncology.2008.10.016.
[55] P. Chen, H. Zuo, H. Xiong, et al., Gpr132 sensing of lactate mediates tumor-macrophage interplay to promote breast cancer metastasis, Proc Natl Acad Sci U S A. 114 (3) (2017) 580–585, https://doi.org/10.1073/pnas.1614035114.
[56] Y.H. You, Z.W. Tian, Z. Du, et al., M1-like tumor-associated macrophages cascade a mesenchymal/stem-like phenotype of oral squamous cell carcinoma via the IL6/Stat3/THBS1 feedback loop, J. Exp. Clin. Cancer Res. 41 (1) (2022) 10, https://doi.org/10.1186/s13046-021-02222-z.
[57] G. Martin-Manso, S. Galli, L.A. Ridnour, et al., Thrombospondin 1 promotes tumor macrophage recruitment and enhances tumor cell cytotoxicity of differentiated U937 cells, Cancer Res. 68 (17) (2008) 7090–7099, https://doi.org/10.1158/0008-5472.CAN-08-0643.
[58] W. Wang, H. Pan, F. Ren, et al., Targeting ASCT2-mediated glutamine metabolism inhibits proliferation and promotes apoptosis of pancreatic cancer cells, Biosci. Rep. 42 (3) (2022) BSR20212171, https://doi.org/10.1042/BSR20212171.
[59] J.M. Kim, Y.N. Im, Y.J. Chung, et al., Glutamine deficiency shifts the asthmatic state toward neutrophilic airway inflammation, Allergy 77 (4) (2022) 1180–1191, https://doi.org/10.1111/all.15121.
[60] X. Jiang, S. Huang, W. Cai, et al., Glutamine-based metabolism normalization and oxidative stress alleviation by self-assembled bilirubin/V9302 nanoparticles for psoriasis treatment, Adv Healthc Mater 12 (13) (2023) e2203397, https://doi.org/10.1002/adhm.202203397.
[61] S. Ming, J. Tian, K. Ma, et al., Oxalate-induced apoptosis through ERS-ROS-NF-κB signalling pathway in renal tubular epithelial cell, Mol Med 28 (1) (2022) 88, https://doi.org/10.1186/s10020-022-00494-5.
[62] M. Oshi, Y. Tokumaru, M. Asaoka, et al., M1 Macrophage and M1/M2 ratio defined by transcriptomic signatures resemble only part of their conventional clinical characteristics in breast cancer, Sci. Rep. 10 (1) (2020) 16554, https://doi.org/10.1038/s41598-020-73624-w.
[63] S. Gao, J. Hu, X. Wu, et al., PMA treated THP-1-derived-IL-6 promotes EMT of SW48 through STAT3/ERK-dependent activation of Wnt/β-catenin signaling pathway, Biomed. Pharmacother. 108 (2018) 618–624, https://doi.org/10.1016/j.biopha.2018.09.067.
[64] W. Su, W. Gao, R. Zhang, et al., TAK1 deficiency promotes liver injury and tumorigenesis via ferroptosis and macrophage cGAS-STING signalling, JHEP Rep 5 (5) (2023) 100695, https://doi.org/10.1016/j.jhepr.2023.100695.